

This is the accepted manuscript made available via CHORUS. The article has been published as:

math

xmlns="http://www.w3.org/1998/Math/MathML">mrow>m
 multiscripts>mi mathvariant="normal">F
 /mi>mprescripts>/mprescripts>none>/none>mn>19/mn>
 /mmultiscripts>msup>mrow>mo>(/mo>mi>p/mi>mo>, /m
 o>mi>γ/mi>mo>)/mo>/mrow>mn>20/mn>/msup>mi>Ne
 /mi>/mrow>/math> and math

xmlns="http://www.w3.org/1998/Math/MathML">mrow>m
 multiscripts>mi mathvariant="normal">F
 /mi>mprescripts>/mprescripts>none>/none>mn>19/mn>
 /mmultiscripts>mo>(/mo>mi>p/mi>mo>, /mo>mi>α/mi>
 mo>)/mo>mmultiscripts>mi
 mathvariant="normal">O/mi>mprescripts>/mprescripts>n
 one>/none>mn>16/mn>/mmultiscripts>/mrow>/math>
 reaction rates and their effect on calcium production in
 Population III stars from hot CNO breakout

R. J. deBoer, O. Clarkson, A. J. Couture, J. Görres, F. Herwig, I. Lombardo, P. Scholz, and M.
 Wiescher

Phys. Rev. C **103**, 055815 — Published 26 May 2021

DOI: [10.1103/PhysRevC.103.055815](https://doi.org/10.1103/PhysRevC.103.055815)

The $^{19}\text{F}(p, \gamma)^{20}\text{Ne}$ and $^{19}\text{F}(p, \alpha)^{16}\text{O}$ reaction rates and their effect on Calcium production in Population III stars from hot CNO breakout

R. J. deBoer,^{1,*} O. Clarkson,^{2,3,4} A.J. Couture,⁵ J. Görres,¹
F. Herwig,^{2,3,4} I. Lombardo,⁶ P. Scholz,¹ and M. Wiescher¹

¹*The Joint Institute for Nuclear Astrophysics, Department of Physics,
University of Notre Dame, Notre Dame, Indiana 46556 USA*

²*Department of Physics & Astronomy, University of Victoria, Victoria, BC, V8W 2Y2, Canada*

³*Joint Institute for Nuclear Astrophysics, Center for the Evolution of the Elements,
Michigan State University, East Lansing, MI 48824, USA*

⁴*NuGrid collaboration*

⁵*Los Alamos National Laboratory, Los Alamos, New Mexico 87545, USA*

⁶*INFN, Sezione di Catania, Via Santa Sofia 64, I-95123 Catania, Italy*

First generation, or Population III, stars have a different evolution than those of later generations owing to their initial primordial abundance composition. Most notably, the lack of carbon, oxygen, and nitrogen, means that primordial massive stars must rely on the less efficient p - p chains, thereby requiring the star to contract to reach temperatures high enough to eventually trigger 3α -reactions. Even small amounts of the $^{12}\text{C}(\alpha, \gamma)^{16}\text{O}$ reactions begin feeding the CNO mass range and enable the CNO cycle to generate energy, but this occurs at higher temperature compared to later stellar generations. It is currently controversial if the observed enhanced abundances of Ca in the most metal-poor stars could be a result of the high temperature H-burning conditions in the first massive stars. The level of this enrichment depends on the hot breakout path from the CNO cycles via the $^{19}\text{F}(p, \gamma)^{20}\text{Ne}$ reaction. In this work, the rates of both the $^{19}\text{F}(p, \gamma)^{20}\text{Ne}$ and competing $^{19}\text{F}(p, \alpha)^{16}\text{O}$ reactions are re-evaluated using the phenomenological R -matrix approach, simultaneously considering several $^{19}\text{F}(p, \gamma)^{20}\text{Ne}$, $^{19}\text{F}(p, \alpha)^{16}\text{O}$, and $^{19}\text{F}(p, p)^{19}\text{F}$ data sets, in order to better characterize the rate uncertainties. It is found that the rate uncertainty for $^{19}\text{F}(p, \gamma)^{20}\text{Ne}$ reaction is considerably larger than previously reported. This is the result of undetermined interferences between observed resonances, a possible threshold state, possible subthreshold states, direct capture, and background levels. Additional experimental measurements are therefore needed to determine if $^{19}\text{F}(p, \gamma)^{20}\text{Ne}$ CNO breakout is responsible for Ca enrichment in metal poor stars. Astrophysically, the breakout reaction revision makes it less likely that Ca observed in the most Fe-poor stars can originate in hot CNO breakout H-burning nucleosynthesis, thereby casting doubt on the prevailing faint supernova scenario to explain the abundances observed in these stars.

I. INTRODUCTION

A fundamental question in nuclear astrophysics concerns the reaction flow out of the CNO cycles towards heavier masses in hydrogen burning environments. At low temperature hydrogen burning, such as in massive main sequence stars, and even in low temperature cataclysmic events, such as in classical novae, the CNO matter remains in the mass range below $A \approx 20$. The initial abundance distribution of the CNO isotopes change depending on the temperature density regime of the nucleosynthesis event. Only in explosive hydrogen at burning temperatures sufficiently in excess of ≈ 0.3 GK, can break-out from the CNO cycles occur via the $^{15}\text{O}(\alpha, \gamma)^{19}\text{Ne}$ and $^{18}\text{Ne}(\alpha, p)^{21}\text{Na}$ reactions, triggering a thermonuclear runaway via the αp -process. The required temperatures for break-out are anticipated for accreting neutron stars, triggering an X-ray burst as an observable event and are also possible for high temperature nova events associated with accreting white dwarfs. A summary of these break-out scenarios has been dis-

cussed before by Wiescher *et al.* [1] and multiple experiments, using a wide range of experimental techniques, have been performed to determine the reaction rates of the α induced break-out reactions $^{15}\text{O}(\alpha, \gamma)^{19}\text{Ne}$ [2–7] and $^{18}\text{Ne}(\alpha, p)^{21}\text{Na}$ [8–12].

Little attention has been given to the $^{19}\text{F}(p, \gamma)^{20}\text{Ne}$ reaction as a possible link between the CNO cycles, the Ne-Na cycles, and possibly beyond. In particular, at temperatures typical for hydrogen-core or -shell burning in massive main-sequence stars, more investigations are needed. In stars with near solar metallicity, the contribution of this reaction to the production of more massive nuclei is negligible compared to other nuclear production mechanisms. However, hot CNO breakout may play a key role in explaining the observed Ca abundance in the most metal-poor stars that carry the abundance signature from the first massive stars.

The most iron-poor stars we observe in our Milky Way's halo are each believed to display the nucleosynthetic signatures resulting from a single Population III (Pop III) star [13]. Keller *et al.* [14] suggested hot CNO breakout during hydrogen burning as the source of Ca production in the most iron and Ca-poor star known at the time, SMSS0313-6708. The Ca abundance was reported as $[\text{Ca}/\text{H}] = -7.2$ and -6.94 in analysis done by

* Electronic address: rdeboer1@nd.edu

58 Nordlander *et al.* [15] using solar abundances of Asplund
59 *et al.* [16]. Takahashi *et al.* [17] also cite hot CNO break-
60 out to produce Ca in SMSS0313-6708, HE 1327-2326 and
61 HE 0107-5240. HE 1327-2326 and HE 0107-5240 have
62 [Ca/H] values of -5.3 and -5.13, respectively, based on an
63 analysis provided in Collet *et al.* [18], and the same solar
64 composition as above.

65 Using a combination of stellar evolution and single-
66 zone nucleosynthesis calculations, Clarkson and Herwig
67 [19] identified the $^{19}\text{F}(p, \gamma)^{20}\text{Ne}$ reaction as the most im-
68 portant breakout path for hydrogen burning conditions
69 in massive Pop III stars. Clarkson and Herwig [19] in-
70 vestigated the conditions for the hot CNO breakout to
71 produce the observed levels of Ca based on a detailed
72 survey of Pop III massive star simulations with masses
73 ranging from 15 to 140 M_{\odot} , and a range of commonly
74 adopted assumptions on stellar mixing to cover the re-
75 lated systematic uncertainties. They conclude, based on
76 these simulations, that it is unlikely that large amounts
77 of Ca can be produced by hot CNO breakout. Even un-
78 der the most optimistic assumptions of the mixing and
79 ejection mechanisms, the predicted Ca abundance is be-
80 tween ≈ 0.8 and nearly 2 dex lower than required by ob-
81 servations of the most metal-poor stars. However, they
82 also note that if the $^{19}\text{F}(p, \gamma)^{20}\text{Ne}/^{19}\text{F}(p, \alpha)^{16}\text{O}$ reaction
83 rate ratio were a factor of ≈ 10 higher than that reported
84 in the NACRE compilation [20], the model predictions of
85 hot H burning may be able to account for the observed
86 Ca abundances in metal-poor stars.

87 Based on the presently available nuclear data, the find-
88 ings of Clarkson and Herwig [19] are in conflict with the
89 previous assertions that the observed Ca in the most
90 metal-poor stars originates in H burning. The question
91 has far-reaching consequences for how the first stars are
92 believed to evolve and die. If Ca can be produced from
93 H burning, then Ca produced in the later Si-burning
94 phases can fall back into the supernova, which is a key
95 ingredient in the prevailing faint supernova with efficient
96 fallback scenario. If Ca cannot be produced in hot H
97 burning, then a new mechanism is needed. Either the
98 supernova scenario has to be revised, or an alternative
99 source must be validated. Other potential sources in-
100 clude a convective-reactive light Pop III *i*-process [21] or
101 Ca synthesis from explosive burning.

102 As described in Wiescher *et al.* [1], the possibility
103 of a break-out from the cold CNO cycles depends on
104 the feeding of ^{19}F from the equilibrium abundances
105 of ^{17}O and ^{18}O in the third cycle. Leakage via
106 the $^{19}\text{F}(p, \gamma)^{20}\text{Ne}$ reaction would cause an irreversible
107 flow from the CNO to the NeNa range because back-
108 processing via $^{22}\text{Ne}(p, \alpha)^{19}\text{F}$ is energetically impossible.
109 The leakage not only depends on the abundance of ^{19}F
110 but also on the reaction rates of $^{19}\text{F}(p, \gamma)^{20}\text{Ne}$ and the
111 competing back-processing reaction $^{19}\text{F}(p, \alpha)^{16}\text{O}$. There-
112 fore, the ratio of the $^{19}\text{F}+p$ reactions is also of critical
113 importance in understanding the production of Ca in the
114 second generation stars observed today.

115 The compound nucleus of both reactions, ^{20}Ne , is char-

acterized by a pronounced α cluster structure [22], which
116 favors the α -emission of the $^{19}\text{F}+p$ resonance states to
117 ^{16}O final states over the decay via γ -emission to bound
118 states in ^{20}Ne . Traditionally, the $^{19}\text{F}(p, \alpha)^{16}\text{O}$ reaction
119 is estimated to be three to four orders of magnitude
120 stronger compared to the $^{19}\text{F}(p, \gamma)^{20}\text{Ne}$ radiative capture
121 reaction [23] (see Fig. 1).
122

123 The experimental confirmation of the predicted reac-
124 tion rates for both reaction channels was troubled for
125 the longest time by a lack or insufficiency of experimen-
126 tal data. Despite several efforts to measure the cross
127 sections, remarkably little has been published. The re-
128 actions $^{19}\text{F}(p, \alpha_0)^{16}\text{O}$ and $^{19}\text{F}(p, \alpha_{(2,3,4)})^{16}\text{O}$ have been
129 measured extensively in the low energy range by Lorenz-
130 Wirzba [24] between $E_p = 0.140.90$ MeV (with data pub-
131 lished by Herndl *et al.* [25]) and by Ott [26] between
132 $E_p = 0.201.64$ MeV, but the majority of these experimen-
133 tal results are not published in peer reviewed articles.

134 More recently, Dababneh *et al.* [27], Spyrou *et al.* [28],
135 Spyrou *et al.* [29], and Couture *et al.* [30] have made
136 additional measurements of the $^{19}\text{F}(p, \alpha_{(2,3,4)})^{16}\text{O}$ reac-
137 tions, largely confirming previous results but significantly
138 improving measurement precision. However, recent di-
139 rect measurements by Lombardo *et al.* [31, 32] and via
140 the Trojan Horse method (THM) by LaCognata *et al.*
141 [33, 34] and Indelicato *et al.* [35], have observed an en-
142 hancement in the low energy $^{19}\text{F}(p, \alpha_0)^{16}\text{O}$ cross section.
143 Strikingly, there have been no modern measurements of
144 the $^{19}\text{F}(p, \alpha_1)^{16}\text{O}$ reaction at low energies.

145 Experimental information is sparse about the compet-
146 ing $^{19}\text{F}(p, \gamma)^{20}\text{Ne}$ reaction which would trigger the break-
147 out from the CNO cycles. The measurements are dif-
148 ficult because of the enormous background count rate
149 from the $^{19}\text{F}(p, \alpha_{(2,3,4)})^{16}\text{O}$ reaction. The presently tab-
150 ulated reaction rate is rather outdated and carries sub-
151 stantial uncertainties [20]. The rate is based primarily on
152 a low-energy study of the $^{19}\text{F}(p, \gamma)^{20}\text{Ne}$ reaction by Sub-
153 oti *et al.* [36] in the energy range between 0.30–1.20 MeV.
154 However, it should be noted that significantly different
155 resonance strengths were found in many cases between
156 Suboti *et al.* [36] and the previous measurements by Far-
157 ney *et al.* [37], Keszthelyi *et al.* [38] and Berkes *et al.*
158 [39]. A recent measurement using the *Q*-value gating
159 technique measured the dominant (p, γ_1) branch of the
160 cross section between 200 and 760 keV [30]. While the
161 low energy resonance at $E_{c.m.} = 213$ keV was not ob-
162 served, an upper limit of $\omega\gamma = 60$ meV was established.
163 The resonance strengths for the other resonances were
164 generally smaller than those previously reported, and the
165 net interference effect at low energies was seen to be de-
166 structive.

167 There is also very limited experimental information
168 available regarding threshold states, subthreshold states,
169 and direct capture strengths. Betts *et al.* [40] reported
170 a 1^+ state near threshold via the $^{19}\text{F}(^3\text{He}, d)^{20}\text{Ne}$ reac-
171 tion. Kious [41] then made a more targeted study, with
172 the $^{19}\text{F}(p, \alpha)^{16}\text{O}$ reaction specifically in mind. They ob-
173 served the same state found by Betts *et al.* [40], but a

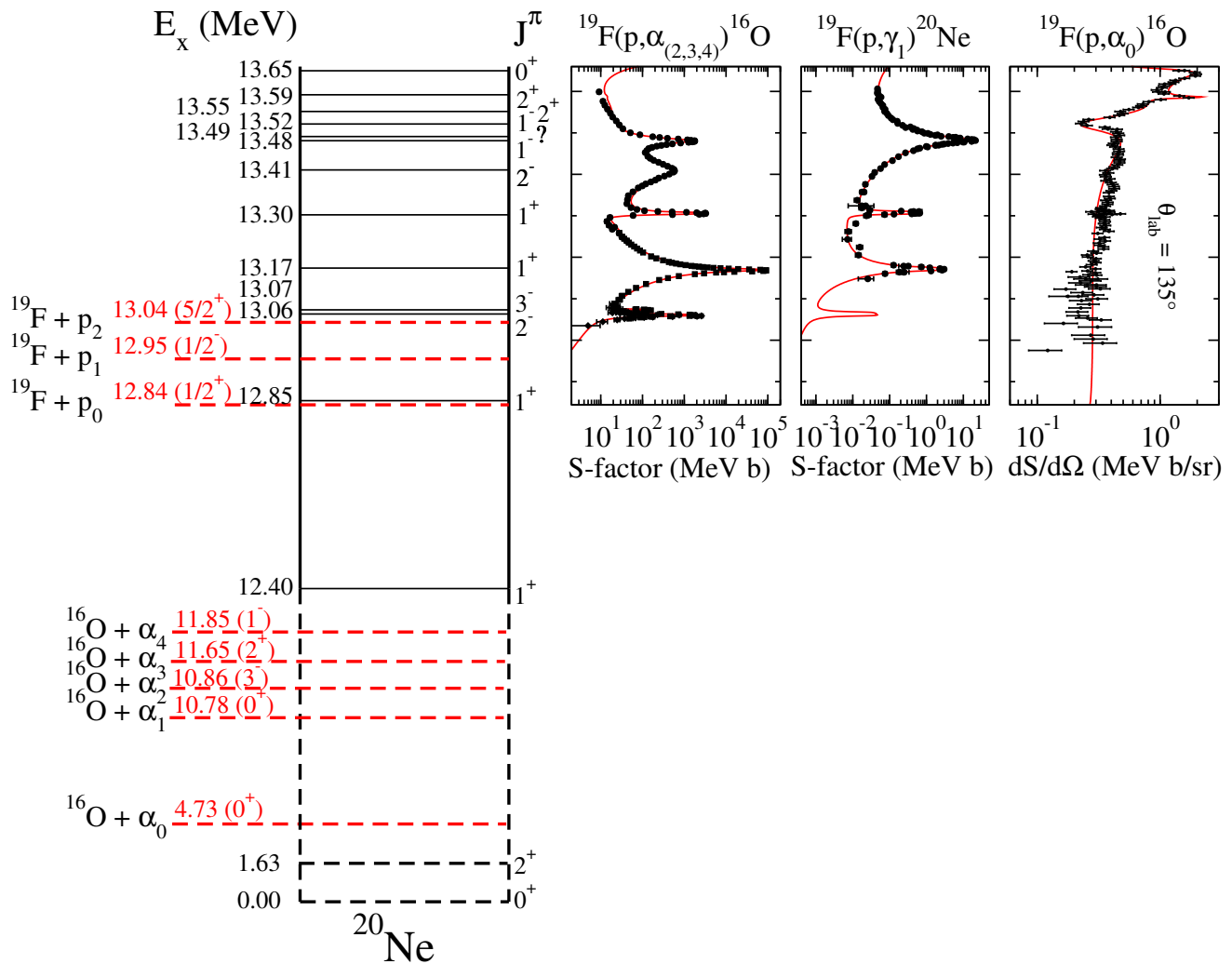


FIG. 1. Level diagram of the ^{20}Ne system, in the vicinity of the proton separation energy, showing the level properties relevant for the present R -matrix analysis of $^{19}\text{F}+p$ reactions. Separation energies are indicated by the red dashed horizontal lines, while levels in ^{20}Ne by black horizontal lines. Note that the lower part of the level diagram, below the real level at $E_x = 12.40$ MeV, is not to scale.

174 more precise determination of the energy was obtained.
 175 Detailed R -matrix calculations were also performed by
 176 Kious [41] in order to demonstrate possible interference
 177 between the near threshold resonance (at $E_p = 11.5$ keV)
 178 and other higher lying resonances for the $^{19}\text{F}(p, \alpha_2)^{16}\text{O}$
 179 reaction. No peer reviewed results have been published
 180 however.

181 This paper seeks to combine these past experimental
 182 results into a more cohesive multichannel R -matrix anal-
 183 ysis [42] that includes all available $^{19}\text{F}+p$ data. This work
 184 begins with a review of the past literature that reports
 185 cross section measurements for the $^{19}\text{F}+p$ reactions in
 186 Sec. II. The data are then subjected to an R -matrix anal-
 187 ysis as described in Sec. III, and systematic uncertainties
 188 are found to dominate. Sec. IV comprises discussions on
 189 several features of the data and the analysis. Based on
 190 these considerations, a revised reaction rate with uncer-
 191 tainty estimates is presented in Sec. V. The implications

192 for the Ca production in Pop III stars are discussed in
 193 Sec. VI while Sec. VII provides a summary.

II. REVIEW OF DATA FROM THE LITERATURE

196 For a comprehensive R -matrix analysis of the
 197 $^{19}\text{F}(p, \alpha)^{16}\text{O}$ and $^{19}\text{F}(p, \gamma)^{20}\text{Ne}$ reactions, ideally, data
 198 for all reactions that populate the ^{20}Ne compound sys-
 199 tem over the excitation energy range of interest should be
 200 included. In this work, previous analyses are improved
 201 on by including the $^{19}\text{F}(p, \alpha_{(0,1,2,3,4)})^{16}\text{O}$, $^{19}\text{F}(p, p_0)^{19}\text{F}$,
 202 and $^{19}\text{F}(p, \gamma_1)^{20}\text{Ne}$ reactions in a simultaneous R -
 203 matrix analysis. Unfortunately no $^{19}\text{F}(p, p_{(1,2)})^{19}\text{F}$ or
 204 $^{19}\text{F}(p, \gamma)^{20}\text{Ne}$ data to other final states are available.
 205 Measurements of these reactions are experimentally possi-
 206 ble and are recommended to improve this type of global

207 analysis in the future. Because of the complexity of several
 208 open channels and high level density, the analysis
 209 has been limited to $E_p \lesssim 0.8$ MeV, which allows for an
 210 accurate calculation of the reaction rate up to ≈ 1 GK.

211 As noted in Sec. I, reactions proceeding through the
 212 $J^\pi = 0^+ \ ^{16}\text{O} + \alpha_{(0,1)}$ channels (see Fig. 1) are limited
 213 to natural parity states, while those going through the
 214 other channels can populate all states in the compound
 215 nucleus. This has the practical consequence that the
 216 $^{19}\text{F}(p, \alpha_0)^{16}\text{O}$ and $^{19}\text{F}(p, \alpha_1)^{16}\text{O}$ cross sections exhibit a
 217 nearly completely different set of resonances and underlying
 218 states than those populated in the $^{19}\text{F}(p, \alpha_{(2,3,4)})^{16}\text{O}$
 219 and $^{19}\text{F}(p, \gamma_{(0,1)})^{20}\text{Ne}$ reactions. In addition, it is important
 220 to note that the first excited state to ground
 221 state decay in ^{16}O can not proceed via γ -ray emission
 222 ($0^+ \rightarrow 0^+$ transition) and instead decays primarily via
 223 pair-production. Therefore, only the $^{19}\text{F}(p, \alpha_{(2,3,4)})^{16}\text{O}$
 224 reactions can be observed through secondary γ -ray emission.
 225 Note that the γ -ray decays of the excited states in
 226 ^{16}O do so with nearly 100% probability directly to the
 227 ground state [43], simplifying secondary γ -ray measure-
 228 ments.

229 It is important to note some alternative notations that
 230 have been used in some previous literature. The most
 231 prolific is the notation $^{19}\text{F}(p, \alpha\gamma)^{16}\text{O}$, which refers to the
 232 $^{19}\text{F}(p, \alpha_{(2,3,4)})^{16}\text{O}$ reactions, emphasizing their detection
 233 via secondary γ -ray emission. A similar alternative nota-
 234 tion, $^{19}\text{F}(p, \alpha_\pi)^{16}\text{O}$, is often used for the $^{19}\text{F}(p, \alpha_1)^{16}\text{O}$
 235 reaction in order to emphasize its primary decay mode
 236 of pair production. It should also be noted that some
 237 early works refer to the $E_x = 6.13$ MeV transition as
 238 the $^{19}\text{F}(p, \alpha_1)^{16}\text{O}$ reaction (see, e.g., the level diagram in
 239 Berkes *et al.* [39]), as it is the first to decay via secondary
 240 γ -ray emission. Since this work primarily uses R -matrix
 241 to analyze each of the reactions individually, the nota-
 242 tion using the individual number of the final state will
 243 be used for clarity.

244 The above nuclear properties rather naturally allow for
 245 the analysis of these different groups of reactions to be
 246 broken up into separate calculations. This was the strat-
 247 egy largely followed in past works, including the recent
 248 work of Lombardo *et al.* [44], where the focus was on the
 249 analysis of the $^{19}\text{F}(p, \alpha_0)^{16}\text{O}$ and $^{19}\text{F}(p, \alpha_1)^{16}\text{O}$ reactions
 250 over a much broader energy range than that investigated
 251 in this work.

A. $^{19}\text{F}(p, \alpha_{(0,1)})^{16}\text{O}$

253 Lombardo *et al.* [44] performed a comprehensive analy-
 254 sis of the $^{19}\text{F}(p, \alpha_{(0,1)})^{20}\text{Ne}$ reactions from near threshold
 255 up to $E_p \approx 10$ MeV and reviews of the relevant litera-
 256 ture covering measurements up to those energies can be
 257 found there. As this work focuses on the low energy
 258 range below $E_p < 0.8$ MeV, the data are limited to those
 259 of Refs. [24, 25, 31, 35, 45–49] for the $^{19}\text{F}(p, \alpha_0)^{20}\text{Ne}$ reac-
 260 tion and Refs. [49, 50] for the $^{19}\text{F}(p, \alpha_1)^{20}\text{Ne}$ reaction.
 261 The data from Ott [26] are also examined but, because

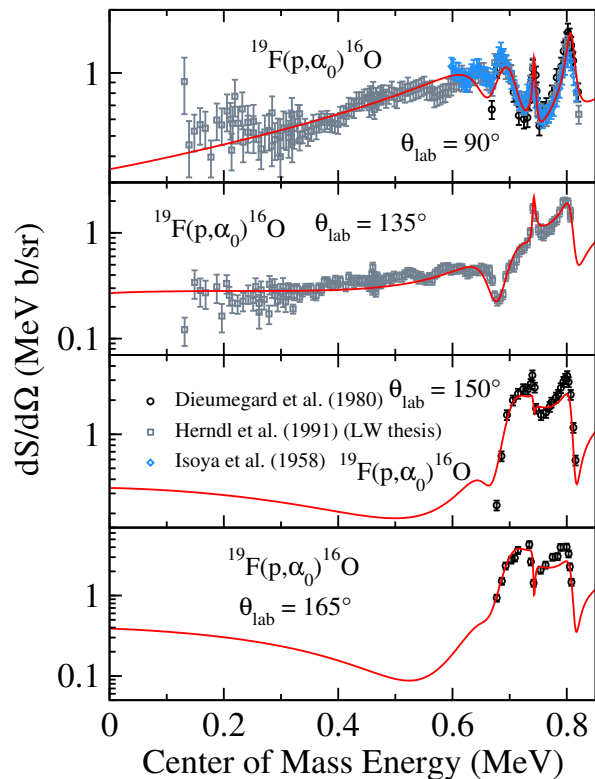


FIG. 2. Differential S -factors of the $^{19}\text{F}(p, \alpha_0)^{16}\text{O}$ data [24, 25, 45, 48].

262 of large experimental effect corrections, the majority of
 263 the data are not included in the present analysis. Data
 264 for the $^{19}\text{F}(p, \alpha_{(0,1)})^{20}\text{Ne}$ reactions considered in the R -
 265 matrix fit are shown in Figs. 2, 3, 4 and 5.

266 As discussed recently in Lombardo *et al.* [44], there is
 267 rather significant inconsistency between the low energy
 268 data of Lombardo *et al.* [32] and that of Lorenz-Wirzba
 269 [24] below $E_{\text{c.m.}} \approx 0.5$ MeV. In this analysis, the data
 270 of Lorenz-Wirzba [24] are fit at low energy to purposely
 271 investigate another fit solution in order to better gauge
 272 the uncertainty in the low energy S -factor. This choice
 273 does not represent a preference of one data set over an-
 274 other. Additional measurements are needed to resolve
 275 this discrepancy.

B. $^{19}\text{F}(p, \alpha_{(2,3,4)})^{16}\text{O}$

277 One of the main focuses of this work is the analysis
 278 of the $^{19}\text{F}(p, \alpha_{(2,3,4)})^{20}\text{Ne}$ reaction channels, which were
 279 not investigated in Lombardo *et al.* [44]. As the corre-
 280 sponding excited states in ^{16}O decay with nearly 100%
 281 probability to the ground state via γ -ray emission, these
 282 reactions are often studied through the detection of sec-
 283 ondary γ -rays. Refs. [24, 29, 30, 38, 39, 51, 52] all include
 284 cross section data for these reactions determined using γ -
 285 ray detection. The data of Devons *et al.* [51] and Spyrou
 286 *et al.* [29] report the sum over all three of these transi-

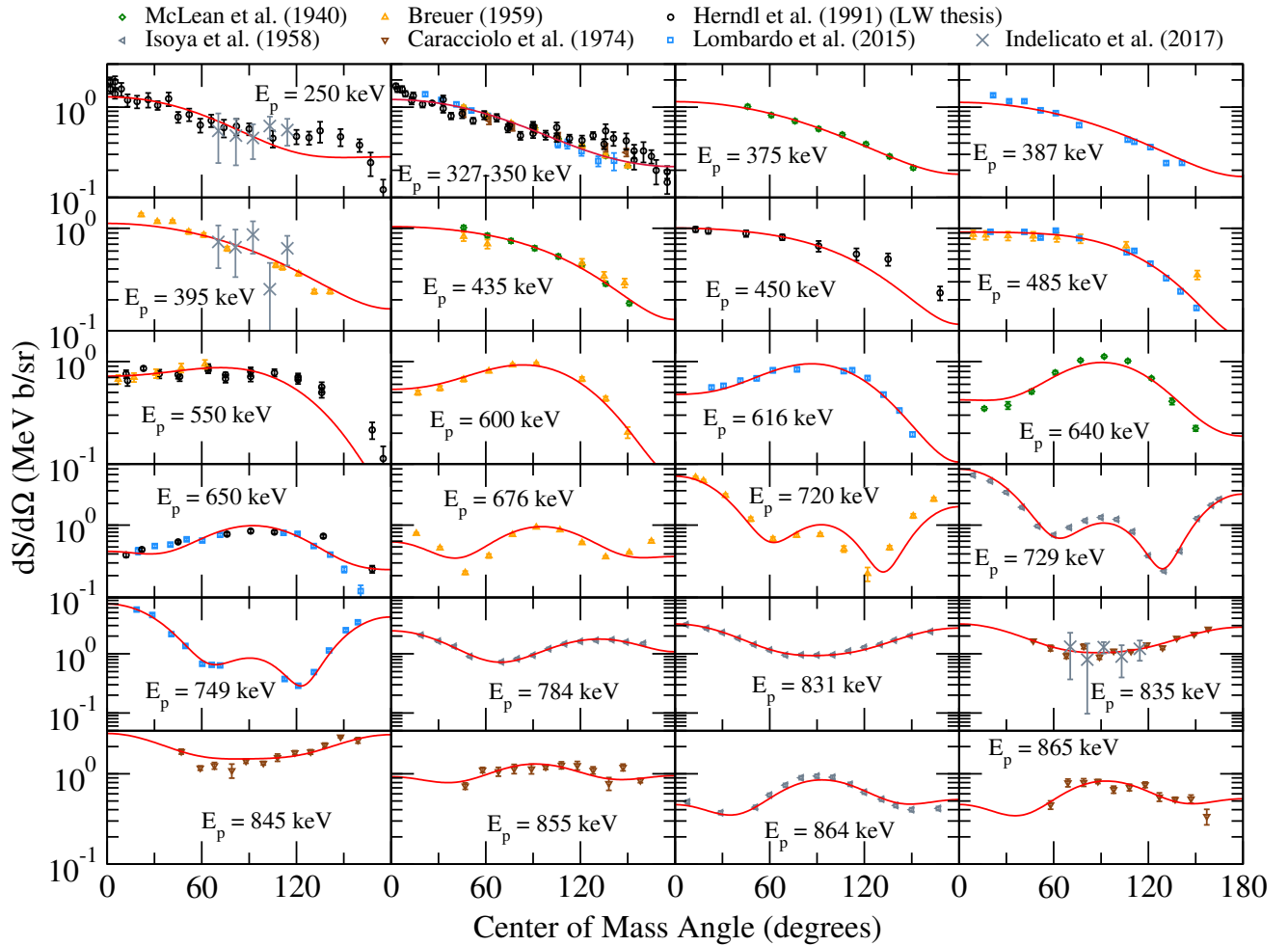


FIG. 3. Low energy angular distributions for the $^{19}\text{F}(p, \alpha_0)^{16}\text{O}$ reaction [24, 25, 32, 35, 46–49].

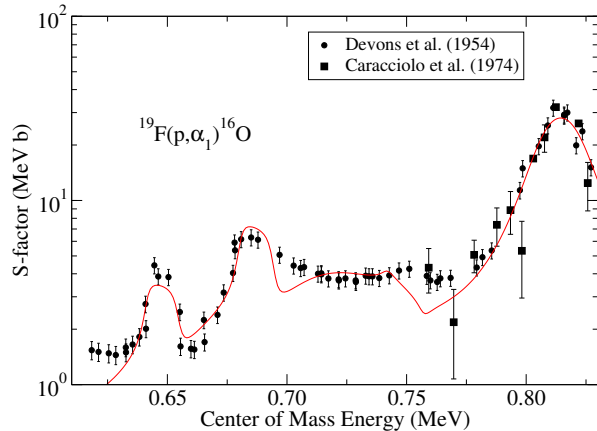


FIG. 4. Lowest energy angle integrated $^{19}\text{F}(p, \alpha_1)^{16}\text{O}$ data of Devons *et al.* [50] and Caracciolo *et al.* [49]. The data of Devons *et al.* [50] has been renormalized as suggested in Lombardo *et al.* [44]. The R -matrix cross section (red line) has been convoluted with the energy resolution of the experiment.

287 tions. The only particle detection experiment is that re-
 288 ported in Ott [26], where a thin gas target was utilized.
 289 The other data sets from Ott [26] are compared with the
 290 fit, but are not included in it, due to the large experimen-
 291 tal effects corrections needed for the thick TaF₅ targets
 292 that were employed. Data for the 6.13 MeV transition
 293 are shown in Figs. 6 and 9, the 6.92 MeV transition in
 294 Fig. 11, and the 7.12 MeV transition in Fig. 12. Fig. 10
 295 shows data for the sum of all three transitions and Figs. 7
 296 and 8 show secondary γ -ray angular distributions.

C. $^{19}\text{F}(p, p_0)^{19}\text{F}$

298 Following Lombardo *et al.* [44], the $^{19}\text{F}(p, p_0)^{19}\text{F}$ data
 299 of Caracciolo *et al.* [49] are included. The current analysis
 300 is expanded to also include the data of Webb *et al.* [53],
 301 where simulation of experimental effects were necessary.
 302 The data are shown in Fig. 13.

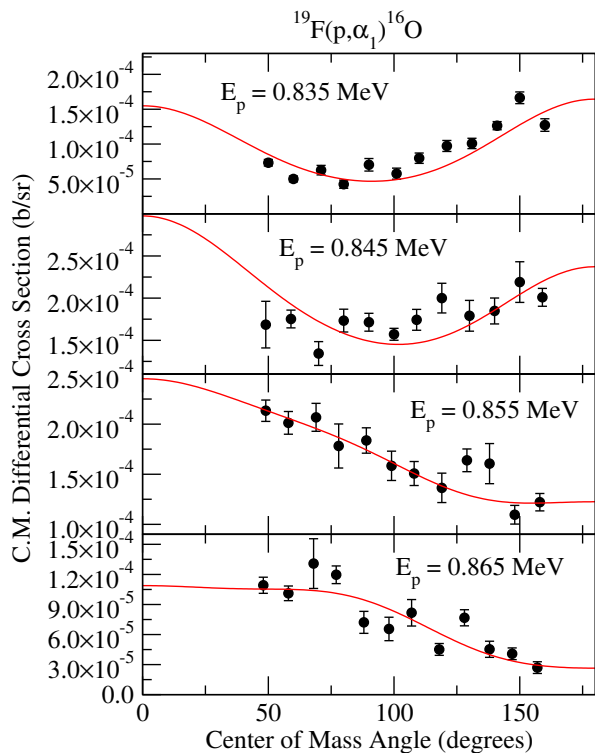


FIG. 5. Angular distributions of the $^{19}\text{F}(p, \alpha_1)^{16}\text{O}$ reaction from Caracciolo *et al.* [49].

D. $^{19}\text{F}(p, \gamma)^{20}\text{Ne}$

Data for the $^{19}\text{F}(p, \gamma)^{20}\text{Ne}$ reaction are very limited. The only cross section data are those of Couture *et al.* [30] and only for the $^{19}\text{F}(p, \gamma_1)^{20}\text{Ne}$ transition. Thick target yield studies of the narrow levels in this region report only small branchings to the ground state as summarized in Table 20.24 of the compilation [54]. The data of Couture *et al.* [30] are shown in Fig. 14.

E. Other Reaction Channels

Ideally, this work would also include a full analysis of the $^{16}\text{O} + \alpha$ reactions over the overlapping excitation energy range. $^{16}\text{O}(\alpha, \alpha_0)^{16}\text{O}$ cross sections over this excitation energy range are reported by Caskey [55] and Mehta *et al.* [56]. However, because of the large difference in the α -particle ($S_\alpha = 4.730$ MeV) and proton separation ($S_p = 12.844$ MeV) energies in ^{20}Ne , the excitation energy range for low energy $^{19}\text{F} + p$ induced reactions corresponds to a high energy range for $^{16}\text{O} + \alpha$ induced reactions. It is thus possible to excite a large number of high spin states in the $^{16}\text{O}(\alpha, \alpha_0)^{16}\text{O}$ reaction, complicating the R -matrix analysis of these reactions.

Additionally, no previous R -matrix analyses of the $^{16}\text{O} + \alpha$ reactions have extended up high enough in energy to exceed S_p . Currently, the low energy range has

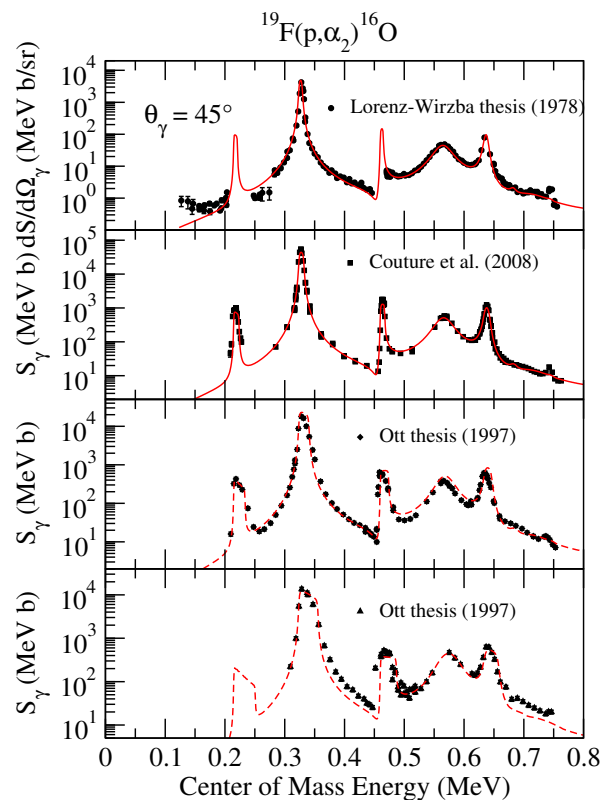


FIG. 6. The R -matrix fit to the $^{19}\text{F}(p, \alpha_2)^{16}\text{O}$ secondary γ -ray data of Lorenz-Wirzba [24] and Couture *et al.* [30] is shown by the red solid line. Additional data from Ott [26], which used substantially thicker targets, was not included in the fit, but calculations are shown (red dashed lines) comparing the R -matrix fit from this work convoluted with the experimental resolution.

been analyzed using R -matrix by Costantini *et al.* [57], focusing on the $^{16}\text{O}(\alpha, \gamma)^{20}\text{Ne}$ reaction. At higher energies, Berthoumieux *et al.* [58] analyzed $^{16}\text{O}(\alpha, \alpha)^{16}\text{O}$ data from $E_\alpha = 3.0$ to 3.4 MeV and more recently Nauruzbayev *et al.* [59] and Hao *et al.* [60] have performed fits to limited sets of data up to $E_\alpha = 6.25$ MeV and $E_\alpha = 9.0$ MeV respectively. However, these higher energy analyses were limited to backward angle data and still do not exceed the proton threshold which corresponds to $E_\alpha = 10.14$ MeV.

As discussed in Lombardo *et al.* [44], of particular interest are the $^{16}\text{O}(\alpha, \alpha_1)^{16}\text{O}$ data of Laymon *et al.* [61]. In that work, a strong 2^+ resonance was identified at $E_\alpha = 10.45$ MeV ($E_x = 13.09$ MeV), which would correspond to $E_p \approx 260$ keV for the $^{19}\text{F}(p, \alpha_1)^{16}\text{O}$ reaction. The general trend of the data can be reproduced with a broad 2^+ state, but it is clear that the angular distribution is distorted from that of an isolated resonance, indicating contributions from other weaker nearby levels. This is shown by the partial wave analysis in Fig. 4 of Laymon *et al.* [61]. Additional measurements are highly desirable for this reaction.

A significant amount of data is also available for the β -

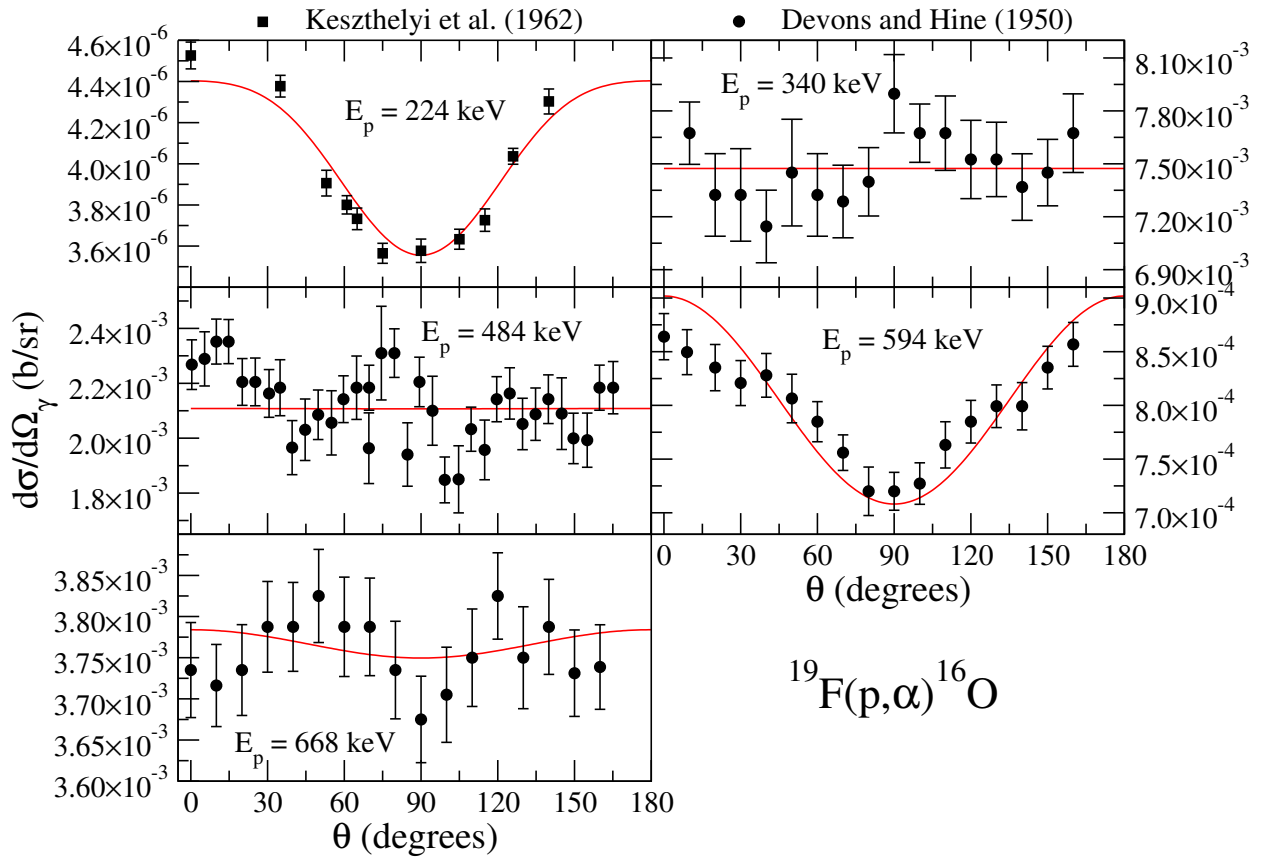


FIG. 7. Secondary on-resonance γ -ray angular distribution measurements for the $^{19}\text{F}(p, \alpha_{(2,3,4)})^{16}\text{O}$ reactions [38, 51]. The data of Devons *et al.* [51] are the sum of the three secondary γ -ray transitions while that of Keszthelyi *et al.* [38] are of only the $^{19}\text{F}(p, \alpha_2)^{16}\text{O}$ reaction.

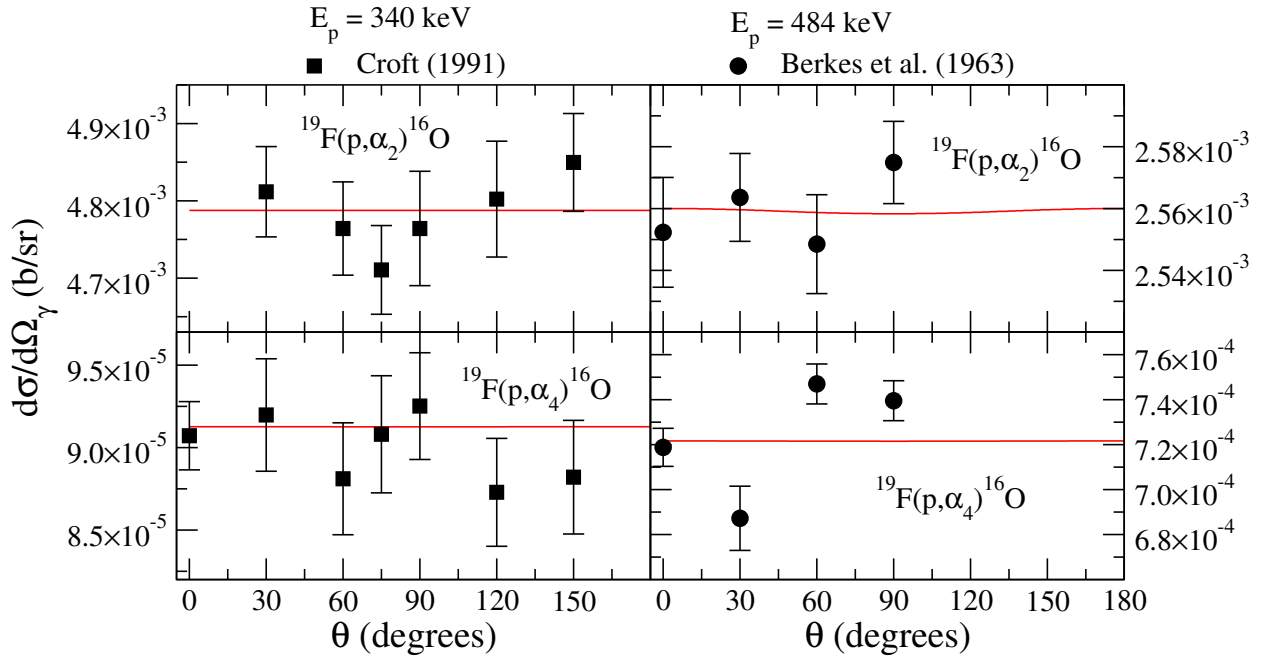


FIG. 8. Secondary on-resonance γ -ray angular distribution measurements for the $^{19}\text{F}(p, \alpha_{(2,4)})^{16}\text{O}$ reactions at $E_p = 340$ keV [52] and 484 keV [39]. The isotropic distributions of these isolated resonances provide accurate relative angular distribution calibrations for γ -ray detectors.

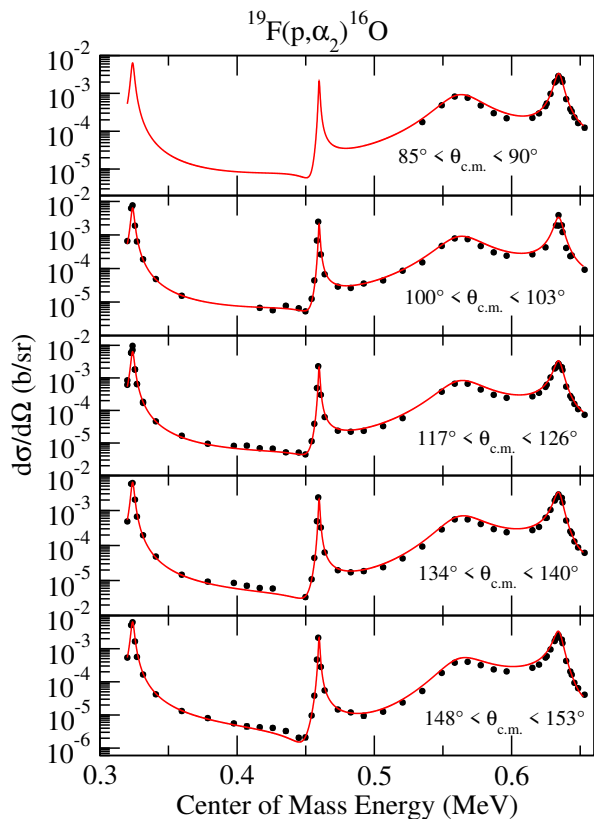


FIG. 9. Differential cross section measurement of the $^{19}\text{F}(p, \alpha_2)^{16}\text{O}$ reaction through observation of the α -particles. This thin target data set from Ott [26] is unique for this reaction, as all others have been made by measuring secondary γ -rays.

350 delayed α decay spectrum of $^{20}\text{Na}(\beta\alpha)^{16}\text{O}$ [62, 63]. The
 351 decay has been observed to proceed strongly through several 2^+
 352 states via allowed transitions. While the cutoff energy is at $E_x = 13.89$ MeV, extending above the proton
 353 separation energy in ^{20}Ne , even the high statistics measurement of Laursen *et al.* [62] only observes decays
 354 up to $E_x \approx 11.9$ MeV. Therefore, while these data could prove quite useful in a global fitting at lower energies,
 355 levels in the present region of interest have not yet been
 356 observed.

F. Transfer Reactions

361 While transfer reaction data is not included directly
 362 in the R -matrix analysis, the level information for near
 363 threshold levels is of vital importance in the extrapolation
 364 of the cross section to the astrophysically relevant energy
 365 region. In this case, a strong 1^+ near-threshold level
 366 has been identified using the $^{19}\text{F}(^3\text{He}, d)^{20}\text{Ne}$ reaction by
 367 Betts *et al.* [40] and Kious [41] at $E_{\text{c.m.}} = 11$ keV. This
 368 resonance has the potential to strongly affect both the
 369 $^{19}\text{F}(p, \alpha_{(2,3,4)})^{16}\text{O}$ and $^{19}\text{F}(p, \gamma)^{20}\text{Ne}$ reactions. In addition,
 370 Kious [41] reports a subthreshold level at $E_{\text{c.m.}} = -$

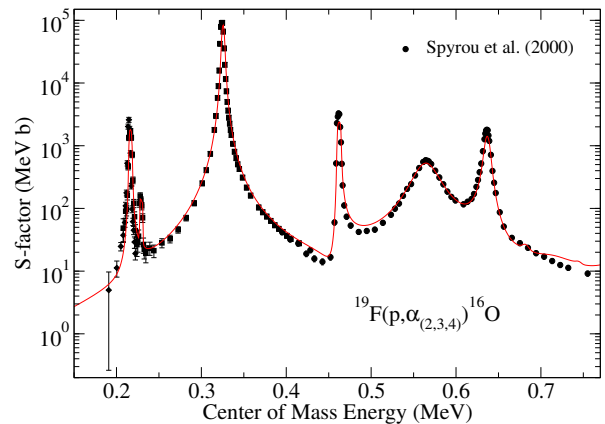


FIG. 10. Sum of the $^{19}\text{F}(p, \alpha_{(2,3,4)})^{16}\text{O}$ reactions measured with a sodium iodide summing detector by Spyrou *et al.* [29]. The R -matrix cross section (red line) has been convoluted with the energy resolution of the experiment.

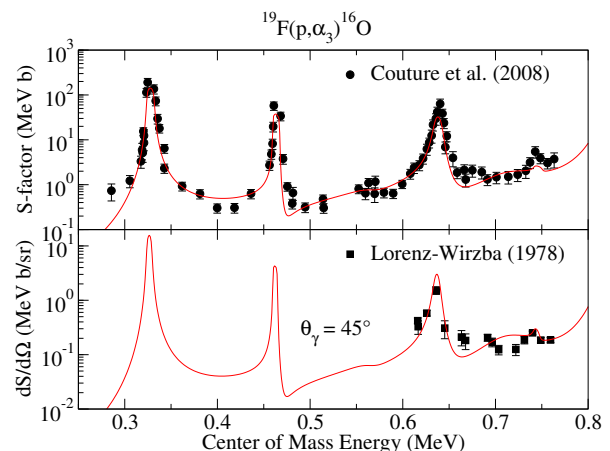


FIG. 11. Experimental data for the $^{19}\text{F}(p, \alpha_3)^{16}\text{O}$ reaction. The top panel displays the angle integrated data of Couture *et al.* [30] (circles) while the bottom panel shows the differential data of Lorenz-Wirzba [24] (squares) at $\theta_\gamma = 45^\circ$. The R -matrix cross section (red line) has been convoluted with the energy resolution of the experiment.

371 448 keV. A dedicated study seems past due in order to
 372 determine the proton ANCs of the bound state levels in
 373 ^{20}Ne to evaluate possible subthreshold resonance contribu-
 374 tions and interference in the low energy cross section.

III. R-MATRIX ANALYSIS

376 Based on the discussions presented in Sec. II,
 377 the present R -matrix analysis includes the reactions
 378 $^{19}\text{F}(p, \alpha_{(0,1,2,3,4)})^{16}\text{O}$, $^{19}\text{F}(p, p_0)^{19}\text{F}$, and $^{19}\text{F}(p, \gamma_1)^{20}\text{Ne}$.
 379 There are no cross section data available to constrain
 380 the branchings to the $^{19}\text{F}(p, p_{(1,2)})^{19}\text{F}$, $^{19}\text{F}(p, \gamma_0)^{20}\text{Ne}$,
 381 or other higher lying γ -ray decay channels. Tilley *et al.*
 382 [54] and Lombardo *et al.* [44] do report some significant

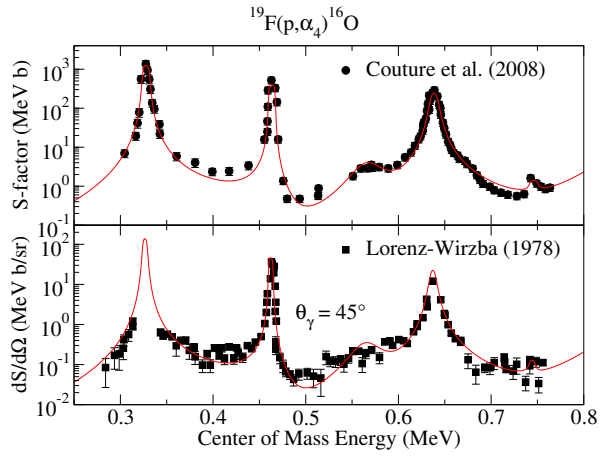


FIG. 12. Experimental data for the $^{19}\text{F}(p, \alpha_4)^{16}\text{O}$ reaction. The top panel displays the angle integrated data of Couture *et al.* [30] (circles) while the bottom panel shows the differential data of Lorenz-Wirzba [24] (squares) at $\theta_\gamma = 45^\circ$. The R -matrix cross section (red line) has been convoluted with the energy resolution of the experiment.

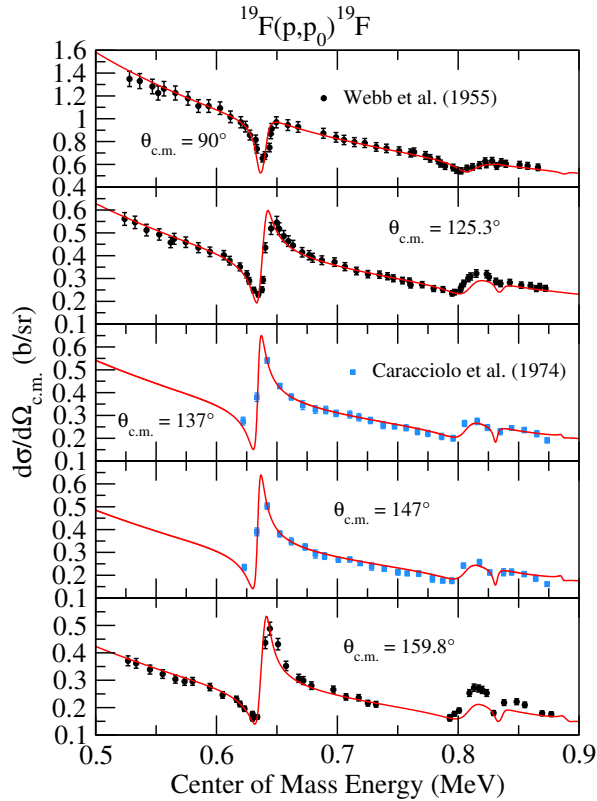


FIG. 13. The limited amount of proton scattering data from Webb *et al.* [53] and Caracciolo *et al.* [49]. The R -matrix cross section (red line) has been convoluted with the energy resolution of the experiment.

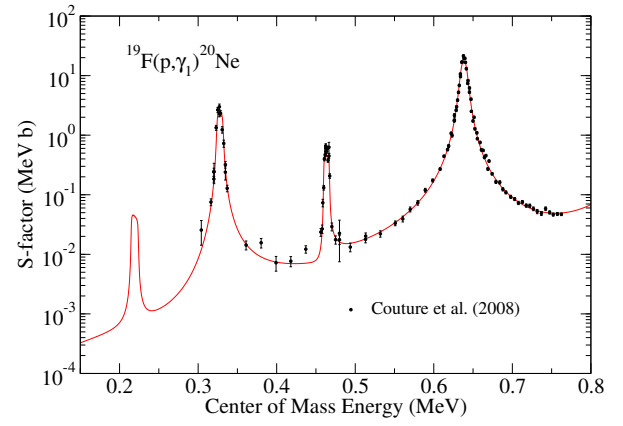


FIG. 14. Only the $^{19}\text{F}(p, \gamma)^{20}\text{Ne}$ data of Couture *et al.* [30] are available for the capture reaction. The R -matrix cross section (red line) has been convoluted with the energy resolution of the experiment.

383 branchings to the $^{19}\text{F}(p, p_{(1,2)})^{19}\text{F}$ channels for the high-
 384 est lying resonance considered in this analysis (see Table II), therefore the p_1 channel is included for this resonance and a background state. It should also be noted
 385 that the present analysis stops just below the multi-
 386 particle breakup threshold, $^{12}\text{C} + 2\alpha$, at $E_x = 13.79$ MeV.

389 For the R -matrix fits, the code AZURE2 [64, 65] has
 390 been used. As is standard for the code, the alternative
 391 R -matrix formalism of Brune [66] is used to work directly
 392 with physical widths and resonance energies. In addition,
 393 a modified version of the code was created that included
 394 the formalism for secondary γ -ray angular distributions
 395 as reported in Brune and deBoer [67] and the ability
 396 to sum the cross sections for multiple reactions (for the
 397 $^{19}\text{F}(p, \alpha_{(2,3,4)})^{20}\text{Ne}$ reaction data of Devons *et al.* [51]
 398 and Spyrou *et al.* [29]). The masses, separation energies,
 399 and channel radii used for the R -matrix fit are given in
 400 Table I. The fit to the data is shown in Figs. 2, 3, 4, 5, 6,
 401 7, 8, 9, 10, 11, 12, 13 and 14 and the best fit parameters
 402 are given in Table II.

403 In general, the R -matrix fit was able to reproduce the
 404 $^{19}\text{F} + p$ data described in Sec. II. For the $^{19}\text{F}(p, \alpha_0)^{16}\text{O}$
 405 data, both the energy and angular dependence of the
 406 low energy cross section was well described as demon-
 407 strated in Figs. 2 and 3. The lowest energy region, below
 408 $E_{c.m.} = 0.65$ MeV, is smoothly varying in energy and the
 409 data could be described using only broad background res-
 410 onances of $J^\pi = 0^+$ and 1^- . In fact, it was possible to
 411 eliminate all of the higher energy levels used in the high
 412 energy fit of Lombardo *et al.* [44], above $E_x = 13.7$ MeV,
 413 and replace their contributions with one or two back-
 414 ground states (see Table II), for each J^π , to simplify the
 415 fitting procedure of the low energy region. The narrow
 416 resonances that are observed in the $^{19}\text{F}(p, \alpha_0)^{16}\text{O}$ data,
 417 above $E_{c.m.} = 0.65$ MeV, were reproduced in a similar
 418 manner as Lombardo *et al.* [32]. It is observed that the
 419 angular distribution data of Lorenz-Wirzba [24] seem to
 420 be systematically above other measurements at backward

TABLE I. Atomic masses (M), particle separation (S), and channel radii (a) used in the R -matrix calculation. Atomic masses are in atomic mass units, separation energies in MeV, and channel radii in fm. Atomic masses and separation energies are taken from Audi *et al.* [68].

Parameter	Value
S_p	12.844 MeV
S_α	4.73 MeV
S_{α_1}	10.779 MeV
S_{α_2}	10.86 MeV
S_{α_3}	11.65 MeV
S_{α_4}	11.85 MeV
M_p	1.0078 u
M_α	4.0026 u
$M(^{16}\text{O})$	15.9949 u
$M(^{19}\text{F})$	18.9984 u
$M(^{20}\text{Ne})$	19.9924 u
$a_{p(0,1,2)}$	5.136 fm
$a_{\alpha(0,1,2,3,4)}$	5.75 fm

angles. There are weak fluctuations at low energy in the $^{19}\text{F}(p, \alpha_0)^{16}\text{O}$ data that may be the result of additional weak resonance contributions, but they are of a similar magnitude as the error bars of the experimental data in that region. As discussed in Sec. II A, the data of [32] are not included in the fit, as well as the two very low energy resonances reported in the THM study of LaCognata *et al.* [33], as they were not needed to reproduce the data that were considered. Further discussions can be found in Sec. IV A.

The limited amount of low energy $^{19}\text{F}(p, \alpha_1)^{16}\text{O}$ data [49, 50] could be described by the same resonances observed over this energy region in the $^{19}\text{F}(p, \alpha_0)^{16}\text{O}$ data (see Figs. 4 and 5), although there are discrepancies between the data and fit in some off-resonance interference regions. The exception is the lowest energy resonance at $E_{c.m.} = 0.63$ MeV ($E_x = 13.48$ MeV) observed in the data of Devons *et al.* [50]. It is possible that this resonance corresponds to the 1^- level that is reported in the literature at $E_x = 13.48$ MeV ($\Gamma = 24(8)$ keV), but the resonance appears to be narrower, with a width of <10 keV. Since no angular distribution information is available in this low energy region, this resonance has been fit using an arbitrary J^π assignment.

Almost none of the natural parity states that contribute strongly to the $^{19}\text{F}(p, \alpha_{(0,1)})^{16}\text{O}$ reactions contribute strongly to the $^{19}\text{F}(p, \alpha_{(2,3,4)})^{16}\text{O}$ reactions or the $^{19}\text{F}(p, \gamma_1)^{20}\text{Ne}$ reaction, which are instead dominated by a shared set of resonances that correspond to unnatural parity states in the ^{20}Ne system. In particular, the cross section is dominated by contributions from only $J^\pi = 1^+$ and 2^- levels. The exceptions are the 2^+ level that is observed as a weak resonance at $E_x = 13.585$ MeV in all the $^{19}\text{F}(p, \alpha_{(0,1,2,3,4)})^{16}\text{O}$ reactions and the $^{19}\text{F}(p, p_0)^{19}\text{F}$

reaction, and the 3^- level that is observed only in the $^{19}\text{F}(p, \alpha_{(2,3,4)})^{16}\text{O}$ sum data of Spyrou *et al.* [29] (see Table II).

Two sets of experimental data dominate the fit for the $^{19}\text{F}(p, \alpha_{(2,3,4)\gamma})^{16}\text{O}$ reactions (see Figs. 6 and 10), the partial cross sections of Couture *et al.* [30] and the γ -ray sum data of Spyrou *et al.* [29]. While Couture *et al.* [30] used a multilevel Breit-Wigner analysis to fit their cross section data, it was found that their parameters resulted in a very good starting point for the R -matrix fit for this reaction.

The data of Spyrou *et al.* [29] were found to be generally consistent with other data sets, especially the higher energy portion of their data. The two other lower energy data sets required a shift of ≈ 6 keV up in energy, even after corrections for target energy loss. However, the shifted data then also agree with the resonance energies quoted in Table 1 of that work. The low energy Spyrou *et al.* [29] data were made with a thin target at these low energies, allowing for the resolution of a new narrow resonance at $E_{c.m.} = 225$ keV, which corresponds to a 3^- level at $E_x = 13.07$ MeV that is just above the previously measured stronger resonance at $E_{c.m.} = 214$ keV corresponding to the 2^- state at $E_x = 13.06$ MeV.

In addition, the thesis data of Lorenz-Wirzba [24], which were published in [25], were also included in the fit. The secondary γ -ray angular distribution formalism of Brune and deBoer [67] was used to fit these differential cross section measurements at $\theta_{\text{lab}} = 45^\circ$. The data include very low energy, thin target, differential cross section measurements for the $^{19}\text{F}(p, \alpha_{(2,4)})^{16}\text{O}$ reactions (see Figs. 6 and 12). While the R -matrix fit was able to accurately reproduce the $^{19}\text{F}(p, \alpha_2)^{16}\text{O}$ differential cross section data of Lorenz-Wirzba [24] over the majority of the energy range, larger discrepancies do occur around the low energy resonance at $E_p = 225$ keV. The increase observed in the low energy cross section data may indicate additional structure at these low energies (see Sec. IV B).

There are also measurements of the $^{19}\text{F}(p, \alpha_{(2,3,4)})^{16}\text{O}$ and $^{19}\text{F}(p, \gamma_1)^{20}\text{Ne}$ reactions given in the unpublished thesis of Ott [26]. The majority of these data sets use thick TaF₅ targets repeating energy ranges already covered by thinner target measurements. The exception to this are the thin gas target differential cross section measurements of the $^{19}\text{F}(p, \alpha_2)^{16}\text{O}$ reaction made through direct α -particle detection. These data are included in the fit and are found to be in good agreement with the other thin target data sets. See further discussion in Sec. IV D.

There are only two sets of low energy $^{19}\text{F}(p, p_0)^{19}\text{F}$ data available in the literature [49, 53] and unfortunately no $^{19}\text{F}(p, p_{(1,2)})^{19}\text{F}$ measurements. The spin assignments of Lombardo *et al.* [44] are adopted and a reasonably consistent fit is obtained. The data of Webb *et al.* [53] required corrections for target resolution and energy loss, which is why they were not used previously in the analysis of Lombardo *et al.* [44].

The experimental $^{19}\text{F}(p, \gamma)^{20}\text{Ne}$ data of Couture *et al.*

TABLE II. R -matrix parameters from the best fit to the $^{19}\text{F}+p$ data considered in this work. Levels marked as “BG” are background levels, and do not correspond to individual levels in the compound system. When two values are given for a partial width, they correspond to either Γ_s/Γ_{s+1} or $\Gamma_\ell/\Gamma_{\ell+1}$, where s and ℓ correspond to the lowest channel spin or orbital angular momentum respectively.

(keV)	(MeV)	(eV)								
$E_{c.m.}$	E_x	J^π	Γ_{p_0}	Γ_{p_1}	Γ_{α_0}	Γ_{α_1}	Γ_{α_2}	Γ_{α_3}	Γ_{α_4}	Γ_{γ_1}
214.9	13.0589	2^-	0.012				1.1×10^3	6.3	1.4	0.06^a
227.9	13.0719	3^-	8.7×10^{-3}				87			
323.9	13.1679	1^+	35.8^a				2.2×10^3	-7.0	62	-0.12
459.9	13.3039	1^+	12.1^a				610	18	-200	0.21
562.7	13.4067	2^-	54				34×10^3	-1.9	-240	-1.0×10^{-3}
634.6	13.4786	1^+	6.5×10^3				-88	2.7	21	1.5
639.9	13.4836	1^-	0.14/-6.8		-87×10^3	-12×10^3	12×10^3			
641.2	13.4852	^b	0.66		4.4×10^3					
681.0	13.5250	1^-	0.88		420	3.6×10^3	150			
709.0	13.5530	2^+	-16/-0.41		39×10^3	-8.9×10^3	-16×10^3	2.9×10^3		
742.4	13.5864	2^+	0.032/0.50		5.2×10^3	-8.4	18		195	
806.5	13.6505	0^+	13×10^3	7.6×10^3	-66	110	0.58			
	13.6752 (BG)	2^-	390/390	780				2.98×10^3		
	13.7300 (BG)	1^+	$5.7 \times 10^3/7.0 \times 10^3$				12	870	780	-1.7/-3.8
	13.8877 (BG) ^d	1^-	590/-590		730×10^3					
	13.9118 (BG) ^d	0^+	-1.4×10^3		390×10^3					
	14.0000 (BG) ^d	2^-	120×10^3					-7.5×10^3		
	20.9409 (BG) ^d	1^-	$1.3 \times 10^8/7.8 \times 10^6$		8.5×10^6	1.7×10^6				

^a Fixed to the value given in Couture *et al.* [30].

^b Spin-parity undetermined.

^c Fixed to the value given in Lombardo *et al.* [44].

^d Fixed

[30] are described well by the levels reported in the literature [54], and are the same as those populated in the $^{19}\text{F}(p, \alpha_{(2,3,4)})^{16}\text{O}$ reactions. As in Couture *et al.* [30], a background 1^+ level was needed to modify the off-resonance interference shape produced by only the levels in the experimentally observed region. Since the data could be reproduced without lower energy resonance or direct capture contributions, these components were not included in the fit. However, their effects on the extrapolation of the cross section to lower energies are discussed in Sec. IV G. The R -matrix fit to the capture data of Couture *et al.* [30] is shown in Fig. 14.

IV. DISCUSSION

A. Inconsistencies between different $^{19}\text{F}(p, a_0)^{16}\text{O}$ and THM measurements

While most of the $^{19}\text{F}(p, a_0)^{20}\text{Ne}$ data from the literature are in good general agreement [69], a significant discrepancy has been observed between the data of Lorenz-Wirzba [24] and Lombardo *et al.* [32]. The data are in reasonable agreement at higher energies above $E_{c.m.} \approx 0.5$ MeV but increasingly diverge at lower en-

ergies, where the data of Lombardo *et al.* [32] are significantly higher in cross section than that of Lorenz-Wirzba [24]. Additionally, the THM measurements of LaCognata *et al.* [33] report two resonances at low energy, which should just overlap the lowest energy data of Lorenz-Wirzba [24]. However, the widths given by LaCognata *et al.* [33] produce a cross section that does not appear to be consistent with the experimental data of Lorenz-Wirzba [24]. Therefore, the main low energy uncertainty in the $^{19}\text{F}(p, a_0)^{20}\text{Ne}$ S -factor results from the systematic differences in these data sets. The data of Lorenz-Wirzba [24] set a lower limit, while the data of LaCognata *et al.* [33] and Lombardo *et al.* [32] give an upper limit as shown in Fig. 15. These discrepancies are considered when determining the uncertainty in the reaction rate as discussed further in Sec. V.

B. The 11 keV threshold resonance

Transfer measurements using the $^{19}\text{F}(^3\text{He}, d)^{20}\text{Ne}$ reaction data [40, 41] have observed a near threshold level at $E_p = 11.5$ keV ($E_x = 12.855$ MeV) [41]. As the level is a 1^+ state, it can only contribute to the $^{19}\text{F}(p, \alpha_{(2,3,4)})^{16}\text{O}$ and $^{19}\text{F}(p, \gamma)^{20}\text{Ne}$ reactions, although it will likely only

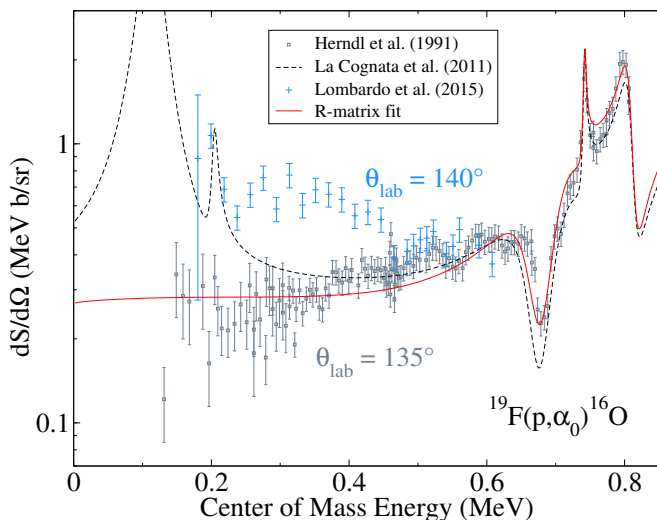


FIG. 15. Illustration of the inconsistencies between the low energy data of Lorenz-Wirzba [24], the data of Lombardo *et al.* [32] and the THM measurements of LaCognata *et al.* [33].

make a significant contribution to the total cross section if its total width is dominated by Γ_{α_2} . The resonance is low enough in energy that it may not contribute to the rate at temperatures of interest, unless its total width is large enough to create significant interference with other higher lying resonances. The total width is highly uncertain [29, 41], both Kious [41] and Spyrou *et al.* [29] have estimated upper limits for the total width based on the proton width determined from the transfer reaction and the resonance's interference with the higher energy off-resonance cross section data. Spyrou *et al.* [29] have estimated an upper limit of 120 eV using a Breit-Wigner analysis, but the present analysis, using a full multilevel R -matrix analysis, found that larger values are possible. The R -matrix analysis reveals that this upper limit is difficult to constrain because the off-resonance cross section over the region of the data could have additional contributions from higher lying resonances and/or subthreshold resonances. The upper limit from the experimental resolution of the transfer measurements is ≈ 1 keV [41], which is consistent with the upper limit estimate from the present R -matrix analysis. In addition, the $^{19}\text{F}(p, \alpha_2)^{16}\text{O}$ data of Lorenz-Wirzba [24] extend to even lower energies than that of Spyrou *et al.* [29] and give a larger cross section than is expected from the R -matrix fit to the higher energy data, even with interference with the near threshold resonance. This may be an indication of other low energy contributions to the cross section.

As shown in Fig. 16, if the near threshold state does have a Γ_{α_2} of ≈ 1 keV it can result in a low energy cross section that is comparable to that of the $^{19}\text{F}(p, \alpha_0)^{16}\text{O}$ cross section, which has been assumed previously to dominate over these low energies [20]. This will also be considered as another source of uncertainty in the reaction rate estimate of Sec. V, as it has a significant effect on

the upper limit.

While it has not been investigated in previous work, given the branching ratios of other nearby states, it is likely that the near-threshold state also has a significant decay branch through γ -ray emission to the first excited state of ^{20}Ne . Fig. 17 shows example interference solutions for the upper limit width estimate ($\Gamma_{\alpha_2} = 1$ keV) of the near threshold state. As will be discussed further in Sec. V, the interference solutions have a significant effect on the (p, γ) reaction rate, due to their large modifications to the low energy cross section.

C. 3^- state observed in Spyrou *et al.* [29]

Spyrou *et al.* [29] observed a narrow low energy resonance at $E_p = 237$ keV on the high energy side of the lowest energy resonance observed at $E_p = 225$ keV in their sum data (see Fig. 10). Due to the close proximity of the two resonances, the only other experiment with similar resolution is that of Lorenz-Wirzba [24]. In that measurement, only data for the $^{19}\text{F}(p, \alpha_2)^{16}\text{O}$ cross section extends low enough in energy to possibly observe the resonance, but the data in this region do not have the sensitivity in yield.

D. Unpublished thesis results

There is a large body of experimental measurements available from experiments at the Universität Stuttgart, which are collected in the thesis of Ott [26]. The majority of these measurements use TaF₅ targets, which are significantly thicker than other measurements. Even when the R -matrix cross section is corrected for target resolution, these measurements deviate somewhat from thin target measurements. This may be the result of the approximations used to convert these data to angle integrated cross sections [26], or could be the result of an insufficiently accurate convolution function given the large corrections necessary. For these reasons, these data were not included directly in the fitting. A comparison of the R -matrix fit with these data, approximately convoluted with the experimental target thickness, is shown in Fig. 6.

The exception to this are the thin target data taken with a gas target system where the differential cross section of the $p(^{19}\text{F}, \alpha_2)^{16}\text{O}$ reaction was determined in inverse kinematics through α -particle detection. This is a unique set of data as nearly all measurements of the $^{19}\text{F}(p, \alpha_2)^{16}\text{O}$ cross section have been made instead by observation of the secondary γ -rays. Further, the excellent agreement of the R -matrix fit with the differential data, as shown in Fig. 9, gives added confidence in the spin-parity assignments of the levels that are populated in this reaction.

The transfer reaction measurements presented in the thesis of Kious [41] provide much of the information available for the near and subthreshold levels that likely play

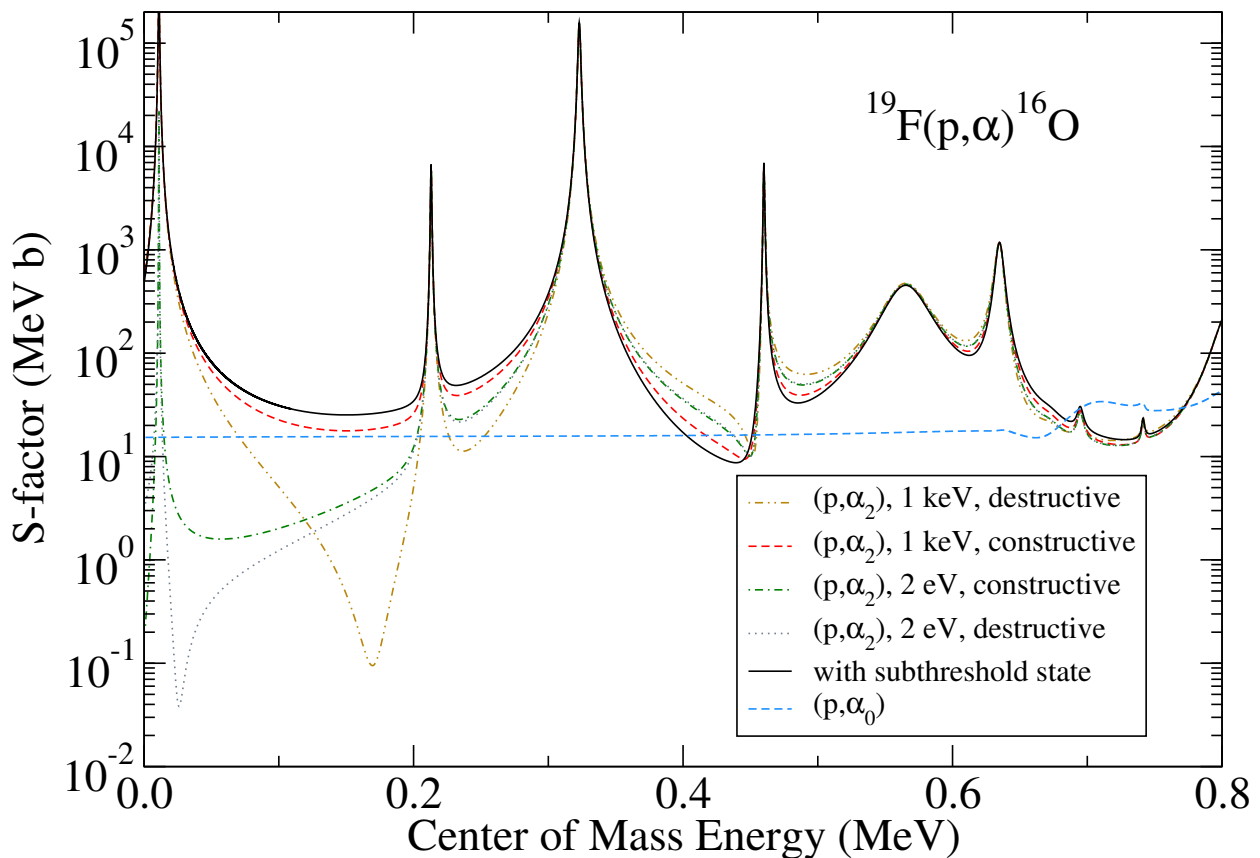


FIG. 16. Calculations of the $^{19}\text{F}(p, \alpha_2)^{16}\text{O}$ S -factor given different interference scenarios and partial width limits for the near-threshold state at 11 keV. These should be compared with the blue dashed line, which corresponds to the nearly constant $^{19}\text{F}(p, \alpha_0)^{16}\text{O}$ S -factor.

643 an important role in the low energy cross section of the
 644 $^{19}\text{F}(p, \alpha_{(2,3,4)})^{16}\text{O}$ and $^{19}\text{F}(p, \gamma)^{20}\text{Ne}$ reactions. This has
 645 already been highlighted for the $^{19}\text{F}(p, \alpha_{(2,3,4)})^{16}\text{O}$ in
 646 Spyrou *et al.* [29]. The importance of the near threshold
 647 state, possible subthreshold contributions, and the lim-
 648 ited previous measurements, provide solid motivations
 649 for new transfer studies.

650 Finally, the data presented in Lorenz-Wirzba [24] are
 651 published in Herndl *et al.* [25], but this work largely
 652 concentrates on comparisons of the data with zero-range
 653 distorted-wave Born approximation calculations and does
 654 not go into any details regarding the measurement of the
 655 experimental data.

656 E. Absolute normalization

657 The absolute normalization of the $^{19}\text{F}(p, \alpha)^{16}\text{O}$ cross
 658 section has proven to be challenging as is evidenced by
 659 the discrepancies in absolute cross sections reported in
 660 different works, which deviate from each other by signifi-
 661 cantly more than their stated uncertainties. One likely
 662 reason is that fluorine targets often experience significant
 663 degradation after only a fraction of a Coulomb of beam

664 bombardment with moderate beam intensities (10's of
 665 μA). Easily made, evaporated LiF targets are too unsta-
 666 ble for the large beam intensities required for low energy
 667 measurements, so CaF_2 or TaF_5 targets have been uti-
 668 lized instead. Even with these more stable targets, large
 669 discrepancies have been reported.

670 For the absolute normalization of the
 671 $^{19}\text{F}(p, \alpha_{(2,3,4)})^{16}\text{O}$ measurements, all other data have
 672 been normalized to those of Couture *et al.* [30], which
 673 were in turn found to be consistent with the strength
 674 measurement of Becker *et al.* [70] for the $E_p = 324$ keV
 675 resonance (see Sec. IV F. For the $^{19}\text{F}(p, \alpha_{0,1})^{16}\text{O}$ data,
 676 the normalization of Lombardo *et al.* [44] has been
 677 adopted. This particular normalization was adopted
 678 because the experiments of Becker *et al.* [70] were specifi-
 679 cally focused on measuring absolute normalizations.
 680 This is reflected in the small uncertainty reported in
 681 their measurement of the $E_p = 340$ keV resonances
 682 strength (see Table IV).

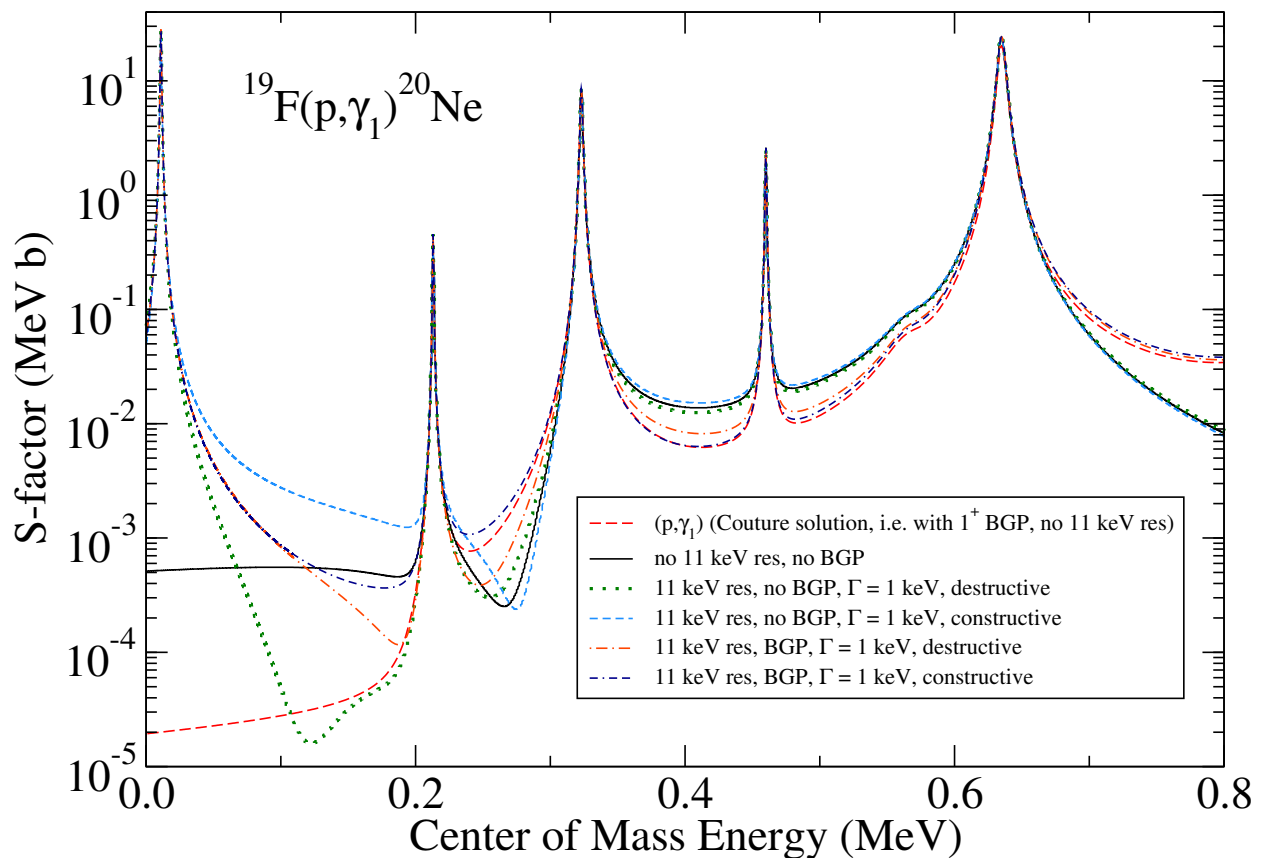


FIG. 17. Calculations of different interference scenarios given the width limitations of the near-threshold state at 11 keV.

F. Comparisons with strength measurements

This work improves on the narrow resonances formalism used by past works as the rate is obtained by numerical integration of the R -matrix cross section. This method allows for the simultaneous and consistent inclusion of both resonance and off-resonance contributions in the reaction rate calculation. Therefore, to compare with previous works, resonance strengths have been calculated based on the partial widths determined by the R -matrix analysis and are given in Tables III and IV.

While the strengths for the $^{19}\text{F}(p, \alpha_{(2,3,4)})^{16}\text{O}$ reactions are generally consistent, those for the $^{19}\text{F}(p, \gamma)^{20}\text{Ne}$ reaction are quite discrepant. Except for the resonance at $E_{r,c.m.} = 0.634$ MeV, the strength measurements for the other resonances typically differ by more than 2σ . It should be noted that in the NACRE compilation [20] average values were adopted for these strengths, despite the large discrepancies.

G. Direct Capture and Subthreshold States

Over the energy region that has been accessed by experimental measurement, the $^{19}\text{F}(p, \gamma)^{20}\text{Ne}$ cross section, at least to the most intense first excited state transition,

is dominated by resonance transitions through unnatural parity states. However, in Couture *et al.* [30], it was shown that there may be a deep interference minimum at lower energies ($E_{c.m.} < 200$ keV). The shape of this interference region is highly dependent on assumptions made about background components from the low energy tails of higher lying resonances, direct capture, and subthreshold state contributions. In particular, direct capture and subthreshold state contributions have seen little experimental investigation.

Only Kious [41] has investigated a possible subthreshold state contribution from a 1^+ level they observed at $E_x = 12.396$ MeV ($S_p = 12.844$ MeV) and only for the (p, α_2) cross section. An example calculation is shown in Fig. 16, where the subthreshold level is given a $\Gamma_{\alpha_2} = 100$ eV ($\theta^2 = 1$) and a proton ANC of $1 \text{ fm}^{-1/2}$ ($\theta^2 = 1 \times 10^{-3}$). Here θ^2 is the dimensionless reduced width (see, e.g., [20]) at the channel radii specified in Table I. These resonance parameters were chosen as they were a combination that gave the maximum value for the $^{19}\text{F}(p, \alpha_2)^{16}\text{O}$ S -factor at low energy, but still produced a higher energy cross section that was consistent with data. It can be seen that the subthreshold state can have a significant impact on the cross section. For example, for a nominal temperature of interest of 0.1 GK, the Gamow energy is 120 keV. At this energy, the variation in the

TABLE III. Comparison of resonance strength measurements for narrow resonances in the $^{19}\text{F}(p, \gamma)^{20}\text{Ne}$ reaction. The uncertainty in the strengths are taken as the systematic uncertainty in the cross section measurement of Couture *et al.* [30] (16%). Table adopted from Angulo *et al.* [20].

$E_{r,c.m.}$ (MeV)	E_x (MeV)	J^π	[71]	[37]	[38]	$\omega\gamma$ (eV)	[39]	[36]	this work	Γ_{p_0} (eV)	Γ_{γ_1} (eV)	Γ_{total} (eV)
0.2148(10)	13.0588	2^-			$1.3(13) \times 10^{-6}$				this work	0.012	<0.06 ^a	1085
0.3239(10)	13.1679	1^+			$3.5(7) \times 10^{-3}$		$10(2) \times 10^{-3}$	$1.4(3) \times 10^{-3}$		35.8 ^b	0.12	2250
0.4599(10)	13.3039	1^+				$5(1) \times 10^{-3}$	$1.6(4) \times 10^{-3}$	$2.3(4) \times 10^{-3}$		12.1 ^b	0.21	834
0.5627(10)	13.4067	2^-				$20(2) \times 10^{-3}$	$5.6(8) \times 10^{-3}$	$<3.9 \times 10^{-3}$		53.6	<2	34600
0.6345(10)	13.4785	1^+	1.58(36)	1.58(36)			1.61(24)	1.1(2)		6480	1.5	6590

^a Fixed at the upper limit of Couture *et al.* [30].

^b Fixed at the value reported in Couture *et al.* [30].

TABLE IV. Comparison of resonance strength measurements for narrow resonances in the $^{19}\text{F}(p, \alpha_{(2,3,4)})^{20}\text{Ne}$ reactions. Note that these resonances strengths only account for the $(p, \alpha_{2,3,4})$ portion of the total cross section at low energies. The uncertainty in the strengths are taken as the systematic uncertainty in the cross section measurement of Couture *et al.* [30] (16%). Table adopted from Angulo *et al.* [20].

$E_{r,c.m.}$ (MeV)	E_x (MeV)	J^π	$\omega\gamma$ (eV)			Γ_{p_0} (eV)	Γ_α (eV)	Γ_{total} (eV)
			[72]	[73]	[29]			
0.011	12.855	1^+			8.5×10^{-29}	$7.5(30) \times 10^{-29}$ [40]	1.1×10^{-28c}	100 - 1000
0.2148(10)	13.0588	2^-		0.022(4)	0.0126(13)		0.012	1090
0.2279(10)	13.0719	3^-			0.011(4)		8.6×10^{-4}	87
0.3239(10)	13.1679	1^+		24(4)	24.3(29)	22.3(8) [70]	35.8 ^b	2250
						22(2) [52]		
						24(3) [74]		
0.4599(10)	13.3039	1^+	10(1)	9(1)	8(1)		12.1 ^b	822
0.5627(10)	13.4067	2^-	52(8)	48(10)	48(7)		54	34600
0.6345(10)	13.4785	1^+	86(13)	90(14)	75(9)		6480	112

^a Fixed at the upper limit of Couture *et al.* [30].

^b Fixed at the central value reported in Couture *et al.* [30].

^c Fixed at the central value reported in Kious [41].

734 S -factor extrapolations, as shown in Fig. 16, is a factor
735 of 17.

733 V. REACTION RATES

734 In this section, the rates, and their correspond-
735 ing upper and lower limits, for the $^{19}\text{F}(p, \gamma)^{20}\text{Ne}$ and
736 $^{19}\text{F}(p, \alpha)^{16}\text{O}$ reactions are calculated based on the R -
737 matrix extrapolations of the S -factors presented in
738 Sec. IV. The rate for the total $^{19}\text{F}(p, \alpha)^{16}\text{O}$ reac-
739 tion is somewhat complicated as it is the sum of the
740 $^{19}\text{F}(p, \alpha_{(0,1,2,3,4)})^{16}\text{O}$ reactions. However, the situa-
741 tion is somewhat simplified because the $^{19}\text{F}(p, \alpha_{(0,2)})^{16}\text{O}$
742 reactions dominate. Similarly, it is possible for the
743 $^{19}\text{F}(p, \gamma)^{20}\text{Ne}$ reaction to proceed through several differ-
744 ent final states, but experimentally the $^{19}\text{F}(p, \gamma_1)^{20}\text{Ne}$
745 transition has been shown to dominate.

746 Ideally the uncertainty of the reaction rates could be
747 calculated through a detailed Bayesian analysis, but, as
748 highlighted throughout Sec. IV, many of the important
749 level parameters for the near and subthreshold states are
750 either very poorly or completely unknown. Thus, with
751 such incomplete knowledge of the priors, this type of de-
752 tailed uncertainty analysis does not seem appropriate.
753 Thus the uncertainties that are quoted here should be
754 treated as classical limits, representing estimates of the
755 extreme upper and lower bounds. Therefore, when these
756 rates are utilized in astrophysics calculations that uti-
757 lize Bayesian uncertainty estimation, it is suggested that
758 the upper and lower limits given here be treated either
759 as the limits of a uniform distribution, or the 3σ values
760 of a normal distribution. The gaps in the experimental
761 data highlighted in this work should serve as motivation
762 for new experimental studies, making a more detailed
763 Bayesian uncertainty analysis of this reaction on the hori-
764 zontal.

765 The individual reaction rates and the upper and lower
766 limits for the dominate components are given in Table V.
767 The total reaction rates are then presented in Table VI.
768 The following sections give further details on how each
769 of the reaction rate components were calculated.

770 A. $^{19}\text{F}(p, \alpha_0)^{16}\text{O}$ rate

771 There have been several recent investigations of the
772 $^{19}\text{F}(p, \alpha_0)^{16}\text{O}$ component of the reaction rate. Measure-
773 ments of the $^{19}\text{F}(p, \alpha_0)^{16}\text{O}$ cross section via THM re-
774 sulted in updated rates as reported in LaCognata *et al.*
775 [33]. The rate was then revised in LaCognata *et al.* [34]
776 based on the new direct measurements of Lombardo *et al.*
777 [32]. New measurements were then made by Indelicato
778 *et al.* [35] reporting the most recent version of the rate
779 based on THM data. Most recently, Lombardo *et al.*
780 [44] has reported a revised rate for the $^{19}\text{F}(p, \alpha_0)^{16}\text{O}$
781 and $^{19}\text{F}(p, \alpha_1)^{16}\text{O}$ components based on a comprehen-
782 sive R -matrix analysis that extends to high energies.

783 Both the new THM measurements [33, 35] and the direct
784 measurements of Lombardo *et al.* [32] indicate a larger
785 $^{19}\text{F}(p, \alpha_0)^{16}\text{O}$ reaction rate than that of older works (in
786 particular of Lorenz-Wirzba [24]), based on the obser-
787 vation of new resonances in the low energy region. In
788 the present work, previous literature data have been re-
789 investigated, which show only a flat low energy cross
790 section without resonant enhancement. This generally
791 agrees with the previous results of Angulo *et al.* [20],
792 which considered mainly the same data sets.

793 Therefore, the uncertainty range for this component
794 of the reaction rate takes the $^{19}\text{F}(p, \alpha_0)^{16}\text{O}$ rate from
795 Lombardo *et al.* [44] as an upper limit and takes the rate
796 of the present analysis as a lower limit. Uncertainties due
797 to the overall normalization of experimental data, which
798 are interpreted to be constant in energy, are also included
799 (see Sec. IV E).

800 B. $^{19}\text{F}(p, \alpha_1)^{16}\text{O}$ rate

801 A revised rate for the $^{19}\text{F}(p, \alpha_1)^{16}\text{O}$ reaction has been
802 presented in Lombardo *et al.* [44], where an enhancement
803 has been indicated due to the presence of a broad 2^+ re-
804 sonance. The rate presented in Lombardo *et al.* [44] is
805 consistent with that found in the present analysis. While
806 there is significant enhancement, the contribution is still
807 less than the $^{19}\text{F}(p, \alpha_0)^{16}\text{O}$ rate contribution at all tem-
808 peratures. This revised rate has been adopted here.

809 C. $^{19}\text{F}(p, \alpha_{(2,3,4)})^{16}\text{O}$ rates

810 One of the main focuses of this work has been a re-
811 evaluation of the $^{19}\text{F}(p, \alpha_{(2,3,4)})^{16}\text{O}$ components of the
812 reaction rate. The data shown that $^{19}\text{F}(p, \alpha_2)^{16}\text{O}$ reac-
813 tion dominates over the entire low energy range for these
814 three reaction components. One of the main results of
815 this work is the demonstration that interference with the
816 1^+ threshold state and subthreshold state can produce
817 a significant enhancement in the $^{19}\text{F}(p, \alpha_2)^{16}\text{O}$ cross sec-
818 tion below the lowest energy observed resonance. With
819 this enhancement the $^{19}\text{F}(p, \alpha_2)^{16}\text{O}$ reaction component
820 could even overshadow the $^{19}\text{F}(p, \alpha_0)^{16}\text{O}$ reaction com-
821 ponent in the low temperature range where it has tradi-
822 tionally been assumed to dominate.

823 D. $^{19}\text{F}(p, \alpha)^{16}\text{O}$ total rate

824 The total $^{19}\text{F}(p, \alpha)^{16}\text{O}$ rate is dominated by the
825 $^{19}\text{F}(p, \alpha_0)^{16}\text{O}$ and $^{19}\text{F}(p, \alpha_2)^{16}\text{O}$ reactions. For the cen-
826 tral value of the rate, the threshold and subthreshold
827 states are not included in the $^{19}\text{F}(p, \alpha_2)^{16}\text{O}$ component.
828 This fit is nearly identical to that presented in Couture
829 *et al.* [30] and is also equivalent over the temperature
830 range under investigation to the narrow width ($\Gamma = 2$ eV)
831 solution shown in Fig. 16. Fig. 18 shows the fractional

TABLE V. Recommended rates (rec) for the $^{19}\text{F}(p, \alpha_{(2,3,4)})^{16}\text{O}$ and $^{19}\text{F}(p, \gamma_1)^{20}\text{Ne}$ reactions as well as a lower limit (low) for the $^{19}\text{F}(p, \alpha_0)^{16}\text{O}$ and lower and upper rate limits (upper) for the $^{19}\text{F}(p, \alpha_2)^{16}\text{O}$ and $^{19}\text{F}(p, \gamma_1)^{20}\text{Ne}$ reactions. See text for details.

T (GK)	(p, α_0) (low)	(p, α_2) (rec)	(p, α_2) (low)	(p, α_2) (up)	(p, α_3) ($\text{cm}^3 \text{mole}^{-1} \text{s}^{-1}$)	(p, α_4)	(p, γ_1) (rec)	(p, γ_1) (low)	(p, γ_1) (up)
0.01	1.66×10^{-24}	4.99×10^{-23}	3.74×10^{-23}	5.73×10^{-23}	4.01×10^{-29}	1.73×10^{-28}	1.10×10^{-28}	1.89×10^{-30}	6.18×10^{-27}
0.02	3.60×10^{-17}	2.20×10^{-16}	1.65×10^{-16}	3.03×10^{-16}	1.10×10^{-21}	4.95×10^{-21}	2.38×10^{-21}	4.13×10^{-23}	3.53×10^{-20}
0.03	1.27×10^{-13}	3.53×10^{-13}	2.65×10^{-13}	5.77×10^{-13}	4.74×10^{-18}	2.23×10^{-17}	8.44×10^{-18}	1.47×10^{-19}	7.04×10^{-17}
0.04	2.17×10^{-11}	3.51×10^{-11}	2.64×10^{-11}	6.77×10^{-11}	9.81×10^{-16}	4.77×10^{-15}	1.44×10^{-15}	2.51×10^{-17}	8.70×10^{-15}
0.05	8.36×10^{-10}	8.85×10^{-10}	6.64×10^{-10}	2.01×10^{-9}	4.53×10^{-14}	2.27×10^{-13}	5.57×10^{-14}	9.64×10^{-16}	3.43×10^{-13}
0.06	1.35×10^{-8}	9.97×10^{-9}	7.48×10^{-9}	2.69×10^{-8}	8.77×10^{-13}	4.49×10^{-12}	8.98×10^{-13}	1.54×10^{-14}	5.67×10^{-12}
0.07	1.24×10^{-7}	6.66×10^{-8}	5.00×10^{-8}	2.15×10^{-7}	9.96×10^{-12}	5.05×10^{-11}	8.25×10^{-12}	1.44×10^{-13}	5.36×10^{-11}
0.08	7.67×10^{-7}	3.13×10^{-7}	2.35×10^{-7}	1.21×10^{-6}	9.31×10^{-11}	3.88×10^{-10}	5.15×10^{-11}	1.11×10^{-12}	3.44×10^{-10}
0.09	3.58×10^{-6}	1.20×10^{-6}	8.97×10^{-7}	5.29×10^{-6}	9.46×10^{-10}	2.31×10^{-9}	2.46×10^{-10}	1.06×10^{-11}	1.67×10^{-9}
0.1	1.35×10^{-5}	4.50×10^{-6}	3.37×10^{-6}	1.98×10^{-5}	9.00×10^{-9}	1.17×10^{-8}	9.93×10^{-10}	1.03×10^{-10}	6.58×10^{-9}
0.15	1.44×10^{-3}	3.87×10^{-3}	2.90×10^{-3}	5.62×10^{-3}	1.88×10^{-5}	2.20×10^{-5}	3.36×10^{-7}	2.41×10^{-7}	1.43×10^{-6}
0.2	2.69×10^{-2}	4.55×10^{-1}	3.41×10^{-1}	4.96×10^{-1}	1.83×10^{-3}	5.49×10^{-3}	2.78×10^{-5}	2.60×10^{-5}	1.31×10^{-4}
0.3	1.04×10^0	9.98×10^1	7.49×10^1	1.02×10^2	3.71×10^{-1}	1.51×10^0	5.63×10^{-3}	5.56×10^{-3}	2.80×10^{-2}
0.4	1.03×10^1	1.45×10^3	1.09×10^3	1.46×10^3	5.65×10^0	2.35×10^1	8.99×10^{-2}	8.92×10^{-2}	4.11×10^{-1}
0.5	5.25×10^1	6.82×10^3	5.12×10^3	6.81×10^3	2.96×10^1	1.21×10^2	6.04×10^{-1}	6.01×10^{-1}	2.32×10^0
0.6	1.83×10^2	1.86×10^4	1.39×10^4	1.84×10^4	9.74×10^1	3.68×10^2	2.90×10^0	2.89×10^0	8.43×10^0
0.7	5.02×10^2	3.73×10^4	2.80×10^4	3.69×10^4	2.71×10^2	8.32×10^2	1.04×10^1	1.04×10^1	2.36×10^1
0.8	1.15×10^3	6.24×10^4	4.68×10^4	6.15×10^4	7.01×10^2	1.58×10^3	2.88×10^1	2.87×10^1	5.56×10^1
0.9	2.32×10^3	9.30×10^4	6.97×10^4	9.12×10^4	1.66×10^3	2.68×10^3	6.41×10^1	6.39×10^1	1.14×10^2
1	4.19×10^3	1.28×10^5	9.59×10^4	1.25×10^5	3.54×10^3	4.20×10^3	1.21×10^2	1.21×10^2	2.10×10^2

TABLE VI. Recommended rates (rec) for the total $^{19}\text{F}(p, \alpha)^{16}\text{O}$ and $^{19}\text{F}(p, \gamma)^{20}\text{Ne}$ reactions as well as lower limit (low) and upper limits (upper) See text for details.

T (GK)	(p, α) (rec)	(p, α) (low)	(p, α) (upper)	(p, γ) (rec)	(p, γ) (low)	(p, γ) (upper)
	($\text{cm}^3 \text{mole}^{-1} \text{s}^{-1}$)					
0.01	1.77×10^{-24}	1.33×10^{-24}	5.90×10^{-23}	1.10×10^{-28}	1.89×10^{-30}	6.18×10^{-27}
0.02	3.78×10^{-17}	2.84×10^{-17}	3.40×10^{-16}	2.38×10^{-21}	4.13×10^{-23}	3.53×10^{-20}
0.03	1.34×10^{-13}	1.01×10^{-13}	7.07×10^{-13}	8.44×10^{-18}	1.47×10^{-19}	7.04×10^{-17}
0.04	2.30×10^{-11}	1.73×10^{-11}	8.99×10^{-11}	1.44×10^{-15}	2.51×10^{-17}	8.70×10^{-15}
0.05	8.87×10^{-10}	6.65×10^{-10}	2.87×10^{-9}	5.57×10^{-14}	9.64×10^{-16}	3.43×10^{-13}
0.06	1.43×10^{-8}	1.07×10^{-8}	4.12×10^{-8}	8.98×10^{-13}	1.54×10^{-14}	5.67×10^{-12}
0.07	1.31×10^{-7}	9.79×10^{-8}	3.53×10^{-7}	8.25×10^{-12}	1.44×10^{-13}	5.36×10^{-11}
0.08	8.13×10^{-7}	6.10×10^{-7}	2.07×10^{-6}	5.15×10^{-11}	1.11×10^{-12}	3.44×10^{-10}
0.09	3.91×10^{-6}	2.93×10^{-6}	9.24×10^{-6}	2.46×10^{-10}	1.06×10^{-11}	1.67×10^{-9}
0.1	1.62×10^{-5}	1.22×10^{-5}	3.42×10^{-5}	9.93×10^{-10}	1.03×10^{-10}	6.58×10^{-9}
0.15	5.58×10^{-3}	5.24×10^{-3}	8.73×10^{-3}	3.36×10^{-7}	2.41×10^{-7}	1.43×10^{-6}
0.2	4.95×10^{-1}	3.95×10^{-1}	6.58×10^{-1}	2.78×10^{-5}	2.60×10^{-5}	1.31×10^{-4}
0.3	9.73×10^1	7.30×10^1	1.22×10^2	5.63×10^{-3}	5.56×10^{-3}	2.80×10^{-2}
0.4	1.39×10^3	1.04×10^3	1.74×10^3	8.99×10^{-2}	8.92×10^{-2}	4.11×10^{-1}
0.5	6.58×10^3	4.93×10^3	8.22×10^3	6.04×10^{-1}	6.01×10^{-1}	2.32×10^0
0.6	1.81×10^4	1.36×10^4	2.26×10^4	2.90×10^0	2.89×10^0	8.43×10^0
0.7	3.70×10^4	2.77×10^4	4.62×10^4	1.04×10^1	1.04×10^1	2.36×10^1
0.8	6.39×10^4	4.79×10^4	7.99×10^4	2.88×10^1	2.87×10^1	5.56×10^1
0.9	9.96×10^4	7.47×10^4	1.25×10^5	6.41×10^1	6.39×10^1	1.14×10^2
1	1.41×10^5	1.09×10^5	1.82×10^5	1.21×10^2	1.21×10^2	2.10×10^2

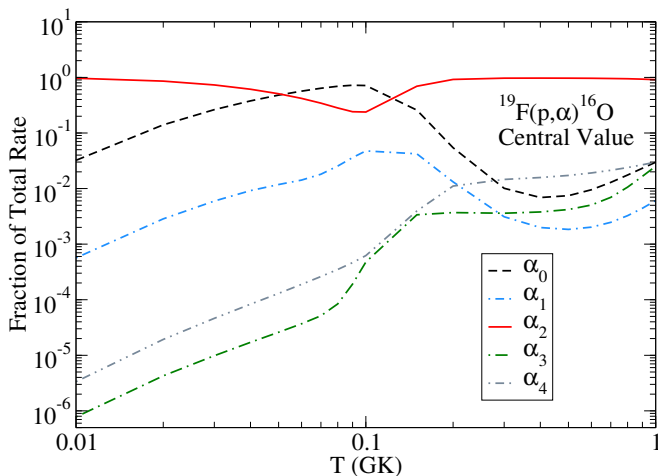


FIG. 18. Fractional contributions of the different final state contributions to the central value calculation of $^{19}\text{F}(p, \alpha)^{16}\text{O}$ reaction rate. Here the $^{19}\text{F}(p, \alpha_0)^{16}\text{O}$ rate dominates around $T \approx 0.1$ GK, as found in previous works (e.g. NACRE [20]).

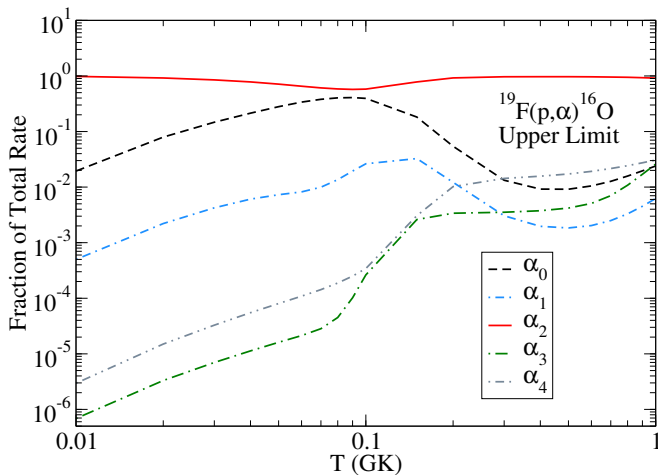


FIG. 19. Fractional contributions of the different final state contributions to the upper limit calculation of $^{19}\text{F}(p, \alpha)^{16}\text{O}$ reaction rate. In this case the interference of the threshold state and subthreshold resonances enhance the $^{19}\text{F}(p, \alpha_2)^{16}\text{O}$ reaction, making it dominant at all temperatures.

832 contribution to the total rate of the different reaction
833 channels for the central value rate.

834 For the upper limit, the interference solution shown
835 by the black line in Fig. 16 is used, where both a broad
836 width is taken for the threshold level ($\Gamma = 1$ keV) and
837 a subthreshold contribution is included. This enhanced
838 $^{19}\text{F}(p, \alpha_2)^{16}\text{O}$ cross section is now larger than even the
839 resonance enhanced rates of the $^{19}\text{F}(p, \alpha_0)^{16}\text{O}$ cross section
840 reported in recent works [35, 44] (as discussed in
841 Sec. V A). The fraction of the total rate stemming from
842 the different reactions is given in Fig. 19. The rate and
843 the recommended uncertainty range are shown in Fig. 20.

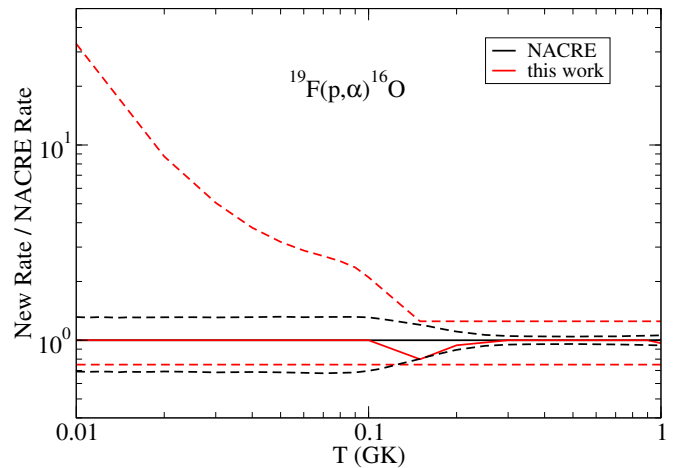


FIG. 20. Ratio of the present reaction $^{19}\text{F}(p, \alpha)^{16}\text{O}$ reaction rate to that of the NACRE compilation [20] (red solid line). The upper and lower uncertainty limits are indicated by the red dashed lines (this work) and the black dashed lines (NACRE [20]).

E. $^{19}\text{F}(p, \gamma)^{20}\text{Ne}$ reaction rate

844
845 One of the other main results of this work has been a
846 re-analysis of the $^{19}\text{F}(p, \gamma)^{20}\text{Ne}$ reaction rate. Here the
847 previous experimental results of Kious [41], Spyrou *et al.*
848 [29], and Couture *et al.* [30] are combined in a global
849 *R*-matrix analysis to gain more insight into the extrap-
850 olation of the low energy cross section. In Angulo *et al.*
851 [20], a 50% uncertainty was adopted for the low tem-
852 perature range for the $^{19}\text{F}(p, \gamma)^{20}\text{Ne}$ reaction. Here it
853 has been shown that, through previously neglected in-
854 terference, the near threshold state and direct capture
855 can result in considerably larger uncertainties, becoming
856 about an order of magnitude at $T = 0.1$ GK and larger
857 than three orders of magnitude at very low temperatures
858 (see Sec. IV and Fig. 21). The effects of this larger un-
859 certainty range are investigated in Sec. VI.

VI. ASTROPHYSICAL IMPACT

861 The details of the suggested CNO breakout in massive
862 Pop III stars are discussed in Clarkson and Herwig [19].
863 Here we will repeat the most salient points and refer the
864 reader to that work for further details.

865 Pop III stars begin their lives with primordial com-
866 position and begin hydrogen burning via $p - p$ chains
867 and contract until central temperatures are high enough
868 ($\approx 10^8$ K) to ignite the 3α -process. This bridges the mass
869 5 and mass 8 gaps, such that a small amount of CNO cat-
870 alyst is formed [75], $X_{12\text{C}} \approx 10^{-9}$, which kickstarts the
871 CNO cycle. In Clarkson and Herwig [19], 1D stellar evo-
872 lution simulations showed that hot CNO cycling takes
873 place at peak core H-burning temperatures although this
874 phase lasts for $\approx 1\%$ of the total main-sequence lifetime.

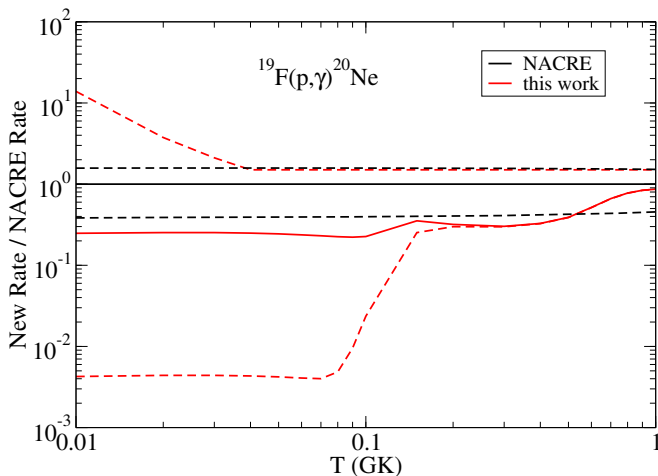


FIG. 21. Ratio of the present reaction $^{19}\text{F}(p, \gamma)^{20}\text{Ne}$ reaction rate to that of the NACRE compilation [20] (red solid line). The upper and lower uncertainty limits are indicated by the red dashed lines (this work) and the black dashed lines (NACRE [20]).

Hot CNO cycles can be activated for a short period of time at the end of hydrogen shell burning in these stars as well. Single-zone nucleosynthesis calculations revealed that small amounts of Ca ($X_{\text{Ca}} \approx 10^{-12}$) are produced through breakout reactions passing through ^{19}F .

To determine the impact of the presented revisions of the $^{19}\text{F}(p, \alpha)^{16}\text{O}$ and $^{19}\text{F}(p, \gamma)^{20}\text{Ne}$ reaction rates, we have run single-zone simulations with the same conditions as those adopted in Clarkson and Herwig [19], which use a constant temperature, $T = 1.19 \times 10^8$ K, and density, $\rho = 39.8 \text{ g cm}^{-3}$, based on their 80 M_{\odot} , Pop III stellar evolution model. Initial abundances are those attributed to the Big Bang abundances [76]. We use the NuGrid collaboration's PPN code [77] with charged-particle reactions from the JINA reaclib V0.5 [78] and $^{19}\text{F} + p$ reactions taken from the NACRE compilation [20], with symmetric uncertainties of 50% as provided. The abundances presented here are measured at the time step where the mass fraction of hydrogen is 10^{-2} . Other single zone calculations using slightly different temperature and density conditions presented in Clarkson and Herwig [19] were also tested with the updated reaction rates but no notable differences in the findings presented below were found.

These simulations show that the new recommended values for these rates decrease the abundances of species with $Z > 9$ (Fig. 22). Mass fractions for these species are quite small in both simulations, with ^{40}Ca being the most abundant, followed by ^{32}S and ^{28}Si . All other mass fractions are $< 10^{-15}$. The updated reaction rates lead to a change of $\approx 70\%$ in these species. Similarly, Fig. 23 shows the change in abundance evolution in our single zone simulations.

Fig. 24 shows the mass fractions of Ca, and the sum of all isotopes with $Z > 9$ in these simulations. The change

in abundance is due almost entirely to the revision of the $^{19}\text{F}(p, \gamma)^{20}\text{Ne}$ reaction rate. The larger uncertainty stems from the investigation of additional uncharacterized reaction contributions to the low energy cross section, namely direct capture, a near threshold state, and subthreshold states (see Secs. IV B and IV G). In the NACRE compilation [20], a non-resonant component was considered, where an estimated uncertainty of 50% was adopted. The total mass fraction of Ca is 2×10^{-13} with the rates presented in this work, and 6.5×10^{-13} using the NACRE rates [20]. Clarkson and Herwig [19] found Ca mass fractions of $\approx 10^{-12}$ in 1D stellar evolution models, somewhat more than what is found in single zone calculations. The difference here is due to the fact that 1D models take into account the continued convective mixing and supply of additional seed CNO material, which is not included in the one-zone simulation. Therefore, the one-zone simulations must be interpreted in a differential sense i.e., the numbers presented here are not intended to be compared with stellar observations directly, but rather show the magnitude of the impact.

As explained in the introduction, Clarkson and Herwig [19] found that model predictions of Ca from H burning sources are ≈ 0.8 to 2 dex too low to account for the observed Ca abundances in the most Fe-poor stars. Repeating the same analysis with the updated reaction rates presented here would increase this tension as the predicted Ca range from H burning decreases by ≈ 0.5 dex. With the updated rates, the models and methods of Clarkson and Herwig [19] would predict H-burning Ca abundances lower by 1.3 to 2.5 dex compared to observations. However, within the range of nuclear uncertainty the predicted Ca abundance approaches the observed Ca abundance within 0.5 dex. More accurate nuclear data is needed to determine the origin of Ca in Pop III stars and thereby distinguish between the faint supernova model and alternative models, such as the light i -process model proposed by Clarkson *et al.* [21], or explosive burning [79].

To summarize, in order to estimate the upper limit of Ca production in the most Fe-poor stars a faint-supernova model has been suggested that requires the fall-back of Ca produced from Si burning, i.e., the Ca produced in these models is not produced during the explosion, and comes from the star's outermost layers. Based on their stellar evolution simulations Clarkson and Herwig [19] find, under these assumptions, an upper limit $[\text{Ca}/\text{H}] = -7.7$, about 0.8 dex below the measured value for the Keller star. The new ^{19}F rates presented here lower the predicted Ca abundance by $\approx 70\%$ at the temperatures present in Pop III H burning (100-150 MK). However, because the uncertainty in the ^{19}F reactions rates is found to be much larger than previously estimated, the updated calculations remain consistent with previous results, clearly indicating the need for additional nuclear data.

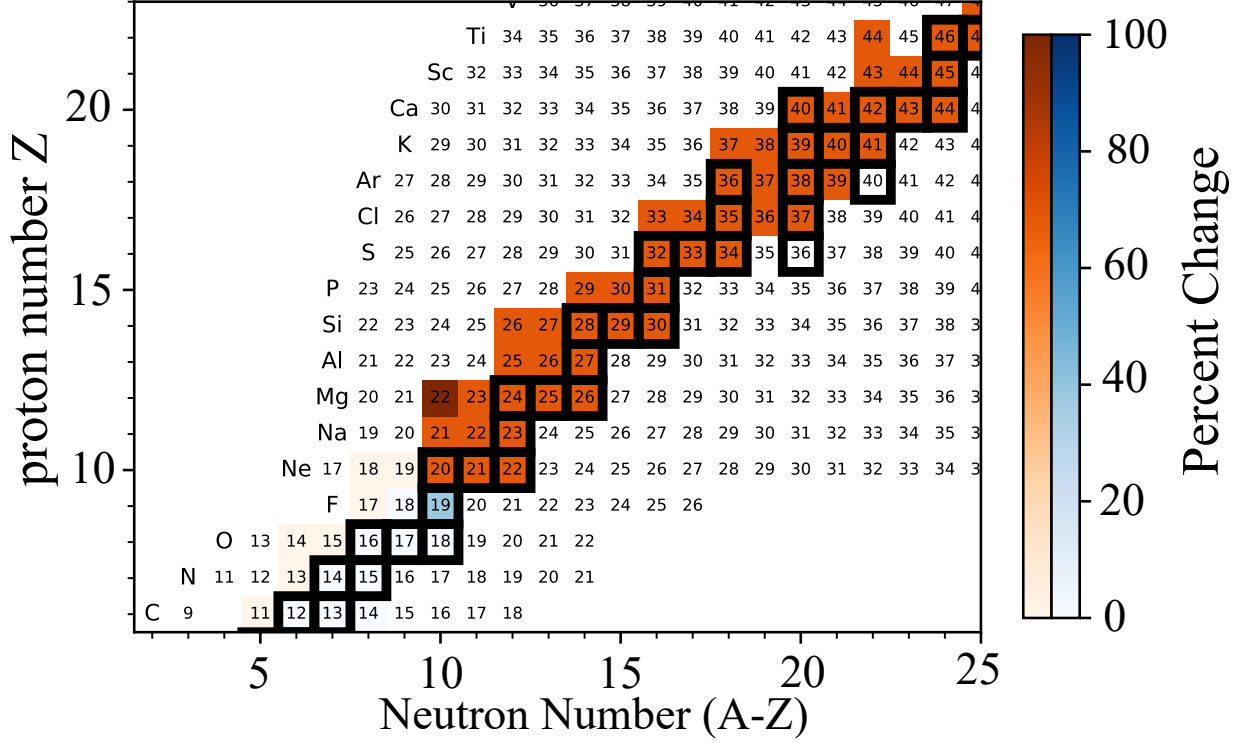


FIG. 22. Abundance chart showing the percent change of isotopes using updated $^{19}\text{F}+p$ reaction rates, presented in this work, compared to rates from the NACRE compilation [20]. Orange colours indicate a reduction in the total mass fractions and blue indicates an increase.

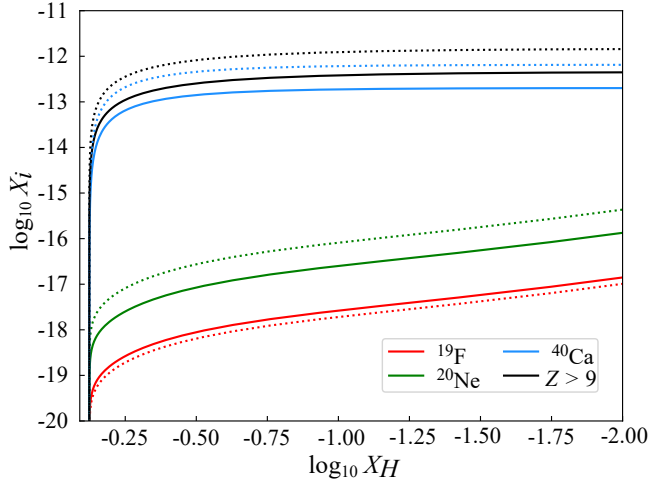


FIG. 23. Abundance evolution showing simulations with rates from this work (solid lines) and using rates from the NACRE compilation [20] for $^{19}\text{F}+p$ reactions (dotted lines). Abundances are plotted as a function of the decreasing amount of H in the single-zone network simulation. Therefore time proceeds from left to right.

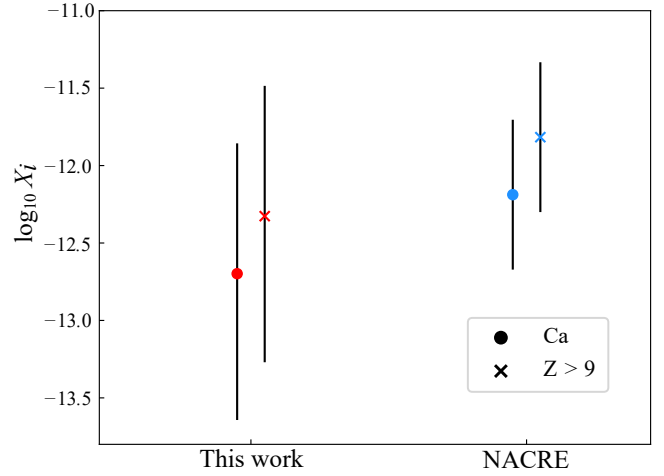


FIG. 24. Mass fractions of Ca, and all isotopes with $Z > 9$ in a Pop III hydrogen burning single zone simulation, calculated using either the $^{19}\text{F}+p$ reaction rates of this work (red) or those from the NACRE compilation [20] (blue). Bars indicate the variation of these abundances within the uncertainties.

VII. SUMMARY

972 cross section data for $^{19}\text{F}+p$ reactions using the phe- 1007
 973 nomenological R -matrix approach. The simultaneous 1008
 974 fit was able to satisfactorily reproduce the available 1009
 975 cross section data for the $^{19}\text{F}(p, \alpha)^{16}\text{O}$, $^{19}\text{F}(p, \gamma)^{20}$, and 1010
 976 $^{19}\text{F}(p, p)^{19}\text{F}$ data. As several recent works have fo- 1011
 977 cused on the $^{19}\text{F}(p, \alpha_{(0,1)})^{16}\text{O}$ reaction, the present work 1012
 978 centers on the $^{19}\text{F}(p, \alpha_{(2,3,4)})^{16}\text{O}$ and $^{19}\text{F}(p, \gamma)^{20}$ reac- 1013
 979 tions. In general, a similar range of uncertainty is found 1014
 980 for the $^{19}\text{F}(p, \alpha)^{16}\text{O}$ reaction rate, but it is found that 1015
 981 the $^{19}\text{F}(p, \alpha_2)^{16}\text{O}$ cross section may be comparable in 1016
 982 strength with the $^{19}\text{F}(p, \alpha_0)^{16}\text{O}$ cross section, even at low 1017
 983 energies where traditionally the $^{19}\text{F}(p, \alpha_0)^{16}\text{O}$ cross sec- 1018
 984 tion has been thought to dominate the total cross section.
 985 It is also found that the uncertainty in the low energy
 986 cross section of the $^{19}\text{F}(p, \gamma)^{20}$ reaction is considerably
 987 larger than previously estimated (e.g. NACRE [20]). 1019

988 These results indicate that further measurements are
 989 needed. Of prime importance, proton transfer studies 1020
 990 should be made in order to determine the proton ANCs 1021
 991 of proton bound states. These are needed both to con- 1022
 992 strain contributions from subthreshold states and to de- 1023
 993 termine the magnitude of the direct capture contribu- 1024
 994 tions for the capture reaction. Measurement of the α_2 - 1025
 995 width of the near threshold state is also also critical. 1026
 996 Low energy measurements of the $^{19}\text{F}(p, p_{(1,2)})^{19}\text{F}$ reac- 1027
 997 tions are also highly desirable in order to better constrain 1028
 998 the multichannel R -matrix analysis. As pointed out in 1029
 999 Couture *et al.* [30], $^{19}\text{F}(p, \gamma_1)^{20}\text{Ne}$ cross section should be 1030
 1000 measured to higher energies in order to better constrain 1031
 1001 high energy resonances contributions. Finally, but likely 1032
 1002 the most difficult, the $^{19}\text{F}(p, \alpha_2)^{16}\text{O}$ and $^{19}\text{F}(p, \gamma)^{20}$ cross 1033
 1003 section measurements need to be extended to lower ener- 1034
 1004 gies, in particular, in their off-resonance regions, in order 1035
 1005 to limit the many different interference solutions that are 1036
 1006 currently possible. In particular, if measurements and 1037

uncertainties for the bound state and near threshold lev-
 els can be made, a more rigorous uncertainty analysis will
 then be appropriate, leading to more statistically mean-
 ingful reaction rate uncertainties.

The larger uncertainty found for the $^{19}\text{F}(p, \gamma)^{20}\text{Ne}$ re-
 action only goes to further emphasize the resulting uncer-
 tainty in nucleosynthesis calculations where these rates
 are needed. The new recommended $^{19}\text{F}(p, \gamma)^{20}\text{Ne}$ rate of
 this work reduces the mass fractions for elements with Z
 > 9 during hydrogen burning in massive Population III
 stars, thus increasing the difficulty in creating Ca solely
 within hydrogen burning conditions in the first stars.

ACKNOWLEDGMENTS

This research utilized resources from the Notre Dame
 Center for Research Computing and was supported by
 the National Science Foundation through Grant No.
 Phys-2011890, and the Joint Institute for Nuclear Astro-
 physics through Grant No. PHY-1430152 (JINA Center
 for the Evolution of the Elements). FH acknowledges
 funding through a NSERC Discovery Grant. This re-
 search has used the Astrohub online virtual research en-
 vironment (<https://astrohub.uvic.ca>) developed and op-
 erated by the Computational Stellar Astrophysics group
 (<http://csa.phys.uvic.ca>) at the University of Victoria
 and hosted on the Computed Canada Arbutus Cloud at
 the University of Victoria. I.L. acknowledges the support
 of the INFN SyLiNuRe grant. A. C. acknowledges sup-
 port from the US Department of Energy (Contract No.
 89233218CNA000001) by the Laboratory Directed Re-
 search and Development program of Los Alamos National
 Laboratory under Project No. LDRD-DR-20190021DR.

1038 [1] M. Wiescher, J. Görres, and H. Schatz, Break-out reac- 1059
 1039 tions from the CNO cycles, *Journal of Physics G: Nuclear*
 1040 *and Particle Physics* **25**, R133 (1999). 1061
 1041 [2] K. Langanke, M. Wiescher, W. A. Fowler, and J. Gorres, 1062
 1042 A new estimate of the $^{19}\text{Ne}(p, \gamma)^{20}\text{Na}$ and $^{15}\text{O}(\alpha, \gamma)^{19}\text{Ne}$ 1063
 1043 reaction rates at stellar energies, *Astrophysical Journal* 1064
 1044 **301**, 629 (1986). 1065
 1045 [3] W. P. Tan, J. L. Fisker, J. Görres, M. Couder, and M. Wi- 1066
 1046 escher, $^{15}\text{O}(\alpha, \gamma)^{19}\text{Ne}$ breakout reaction and impact on 1067
 1047 x-ray bursts, *Phys. Rev. Lett.* **98**, 242503 (2007). 1068
 1048 [4] W. P. Tan, J. Görres, M. Beard, M. Couder, A. Couture, 1069
 1049 S. Falahat, J. L. Fisker, L. Lamm, P. J. LeBlanc, H. Y. 1070
 1050 Lee, S. O'Brien, A. Palumbo, E. Stech, E. Strandberg, 1071
 1051 and M. Wiescher, Measurement of the decay branching 1072
 1052 ratios of the α -unbound states in ^{19}Ne and the $^{15}\text{O}(\alpha, \gamma)$ 1073
 1053 reaction rate, *Phys. Rev. C* **79**, 055805 (2009). 1074
 1054 [5] M. R. Hall, D. W. Bardayan, T. Baugher, A. Lepailleur, 1075
 1055 S. D. Pain, A. Ratkiewicz, S. Ahn, J. M. Allen, J. T. An- 1076
 1056 derson, A. D. Ayangeakaa, J. C. Blackmon, S. Burcher, 1077
 1057 M. P. Carpenter, S. M. Cha, K. Y. Chae, K. A. Chipps, 1078
 1058 J. A. Cizewski, M. Febraro, O. Hall, J. Hu, C. L. Jiang, 1079

K. L. Jones, E. J. Lee, P. D. O'Malley, S. Ota, B. C.
 Rasco, D. Santiago-Gonzalez, D. Seweryniak, H. Sims,
 K. Smith, W. P. Tan, P. Thompson, C. Thornsberrry,
 R. L. Varner, D. Walter, G. L. Wilson, and S. Zhu, New
 γ -ray transitions observed in ^{19}Ne with implications for
 the $^{15}\text{O}(\alpha, \gamma)^{19}\text{Ne}$ reaction rate, *Phys. Rev. C* **99**, 035805
 (2019).
 [6] D. Torresi, C. Wheldon, T. Kokalova, S. Bailey,
 A. Boiano, C. Boiano, M. Fisichella, M. Mazzocco,
 C. Parascandolo, D. Pierroutsakou, E. Strano, M. Zadro,
 M. Cavallaro, S. Cherubini, N. Curtis, A. Di Pietro, J. P.
 Fernández Garcia, P. Figuera, T. Glodariu, J. Grębosz,
 M. La Cognata, M. La Commara, M. Lattuada, D. Men-
 goni, R. G. Pizzone, C. Signorini, C. Stefanini, L. Stroe,
 and C. Spitaleri, Evidence for $^{15}\text{O} + \alpha$ resonance struc-
 tures in ^{19}Ne via direct measurement, *Phys. Rev. C* **96**,
 044317 (2017).
 [7] C. Wrede, B. E. Glassman, D. Pérez-Loureiro, J. M.
 Allen, D. W. Bardayan, M. B. Bennett, B. A. Brown,
 K. A. Chipps, M. Febraro, C. Fry, M. R. Hall, O. Hall,
 S. N. Liddick, P. O'Malley, W.-J. Ong, S. D. Pain,

- 1080 S. B. Schwartz, P. Shidling, H. Sims, P. Thompson, and 1144
 1081 H. Zhang, New portal to the $^{15}\text{O}(\alpha, \gamma)^{19}\text{Ne}$ resonance 1145
 1082 triggering cno-cycle breakout, *Phys. Rev. C* **96**, 032801 1146
 1083 (2017). 1147
- 1084 [8] W. Bradfield-Smith, T. Davinson, A. DiPietro, A. M. 1148
 1085 Laird, A. N. Ostrowski, A. C. Shotton, P. J. Woods, 1149
 1086 S. Cherubini, W. Galster, J. S. Graulich, P. Leleux, 1150
 1087 L. Michel, A. Ninane, J. Vervier, J. Görres, M. Wiescher, 1151
 1088 J. Rahighi, and J. Hinnefeld, Breakout from the hot cno 1152
 1089 cycle via the $^{18}\text{Ne}(\alpha, p)^{21}\text{Na}$ reaction, *Phys. Rev. C* **59**, 1153
 1090 3402 (1999). 1154
- 1091 [9] A. Matic, A. M. vandenBerg, M. N. Harakeh, H. J. 1155
 1092 Wörtche, G. P. A. Berg, M. Couder, J. L. Fisker, 1156
 1093 J. Görres, P. LeBlanc, S. O'Brien, M. Wiescher, K. Fu- 1157
 1094 jita, K. Hatanaka, Y. Sakemi, Y. Shimizu, Y. Tameshige, 1158
 1095 A. Tamii, M. Yosoi, T. Adachi, Y. Fujita, Y. Shimbara, 1159
 1096 H. Fujita, T. Wakasa, P. O. Hess, B. A. Brown, and 1160
 1097 H. Schatz, High-precision (p, t) reaction measurement to 1161
 1098 determine $^{18}\text{Ne}(\alpha, p)^{21}\text{Na}$ reaction rates, *Phys. Rev. C* 1162
 1099 **80**, 055804 (2009). 1163
- 1100 [10] L. Y. Zhang, J. J. He, A. Parikh, S. W. Xu, H. Yam- 1164
 1101 aguchi, D. Kahl, S. Kubono, P. Mohr, J. Hu, P. Ma, S. Z. 1165
 1102 Chen, Y. Wakabayashi, H. W. Wang, W. D. Tian, R. F. 1166
 1103 Chen, B. Guo, T. Hashimoto, Y. Togano, S. Hayakawa, 1167
 1104 T. Teranishi, N. Iwasa, T. Yamada, T. Komatsubara, 1168
 1105 Y. H. Zhang, and X. H. Zhou, Investigation of the ther- 1169
 1106 monuclear $^{18}\text{Ne}(\alpha, p)^{21}\text{Na}$ reaction rate via resonant elas- 1170
 1107 tic scattering of $^{21}\text{Na} + p$, *Phys. Rev. C* **89**, 015804 1171
 1108 (2014). 1172
- 1109 [11] P. J. C. Salter, M. Aliotta, T. Davinson, H. Al Falou, 1173
 1110 A. Chen, B. Davids, B. R. Fulton, N. Galinski, D. How- 1174
 1111 ell, G. Lotay, P. Machule, A. S. Murphy, C. Ruiz, S. Sjue, 1175
 1112 M. Taggart, P. Walden, and P. J. Woods, Measurement 1176
 1113 of the $^{18}\text{Ne}(\alpha, p_0)^{21}\text{Na}$ reaction cross section in the burn- 1177
 1114 ing energy region for x-ray bursts, *Phys. Rev. Lett.* **108**, 1178
 1115 242701 (2012). 1179
- 1116 [12] K. Y. Chae, D. W. Bardayan, J. C. Blackmon, K. A. 1180
 1117 Chipps, R. Hatarik, K. L. Jones, R. L. Kozub, J. F. 1181
 1118 Liang, C. Matei, B. H. Moazen, C. D. Nesaraja, P. D. 1182
 1119 O'Malley, S. D. Pain, S. T. Pittman, and M. S. Smith, 1183
 1120 Constraint on the astrophysical $^{18}\text{Ne}(\alpha, p)^{21}\text{Na}$ reaction 1184
 1121 rate through a $^{24}\text{Mg}(p, t)^{22}\text{Mg}$ measurement, *Phys. Rev.* 1185
 1122 *C* **79**, 055804 (2009). 1186
- 1123 [13] A. Frebel and J. E. Norris, Near-Field Cosmology with 1187
 1124 Extremely Metal-Poor Stars, *Annual Review of Astron-* 1188
 1125 *omy and Astrophysics* **53**, 631 (2015), arXiv:1501.06921 1189
 1126 [astro-ph.SR]. 1190
- 1127 [14] S. C. Keller, M. S. Bessell, A. Frebel, A. R. Casey, 1191
 1128 M. Asplund, H. R. Jacobson, K. Lind, J. E. Norris, 1192
 1129 D. Yong, A. Heger, Z. Magic, G. S. da Costa, B. P. 1193
 1130 Schmidt, and P. Tisserand, A single low-energy, iron- 1194
 1131 poor supernova as the source of metals in the star SMSS 1195
 1132 J031300.36-670839.3, *Nature (London)* **506**, 463 (2014), 1196
 1133 arXiv:1402.1517 [astro-ph.SR]. 1197
- 1134 [15] T. Nordlander, A. M. Amarsi, K. Lind, M. Asplund, 1198
 1135 P. S. Barklem, A. R. Casey, R. Collet, and J. Leenaarts, 1199
 1136 3D NLTE analysis of the most iron-deficient star, 1200
 1137 SMSS0313-6708, *Astronomy & Astrophysics* **597**, A6 1201
 1138 (2017), arXiv:1609.07416 [astro-ph.SR]. 1202
- 1139 [16] M. Asplund, N. Grevesse, A. J. Sauval, and P. Scott, The 1203
 1140 Chemical Composition of the Sun, *Annual Review of Astron-* 1204
 1141 *omy & Astrophysics* **47**, 481 (2009), arXiv:0909.0948 1205
 1142 [astro-ph.SR]. 1206
- 1143 [17] K. Takahashi, H. Umeda, and T. Yoshida, Stellar 1207
 Yields of Rotating First Stars. I. Yields of Weak Su-
 pernovae and Abundances of Carbon-enhanced Hyper-
 metal-poor Stars, *Astrophysical Journal* **794**, 40 (2014),
 arXiv:1406.5305 [astro-ph.SR].
- [18] R. Collet, M. Asplund, and R. Trampedach, The Chem-
 ical Compositions of the Extreme Halo Stars HE 0107-
 5240 and HE 1327-2326 Inferred from Three-dimensional
 Hydrodynamical Model Atmospheres, *The Astrophys-
 ical Journal* **644**, L121 (2006), arXiv:astro-ph/0605219
 [astro-ph].
- [19] O. Clarkson and F. Herwig, Convective H-He Inter-
 actions in Massive Population III Stellar Evolution
 Models, *Monthly Notices of the Royal Astronomical
 Society* 10.1093/mnras/staa3328 (2020), staa3328,
 https://academic.oup.com/mnras/advance-article-
 pdf/doi/10.1093/mnras/staa3328/34042489/staa3328.pdf
- [20] C. Angulo, M. Arnould, M. Rayet, P. Descouvemont,
 D. Baye, C. Leclercq-Willain, A. Coc, S. Barhoumi,
 P. Aguer, C. Rolfs, R. Kunz, J. Hammer, A. Mayer,
 T. Paradellis, S. Kossionides, C. Chronidou, K. Spyrou,
 S. Degl'Innocenti, G. Fiorentini, B. Ricci, S. Zavatarelli,
 C. Providencia, H. Wolters, J. Soares, C. Grama,
 J. Rahighi, A. Shotton, and M. L. Rächti, A compila-
 tion of charged-particle induced thermonuclear reaction
 rates, *Nucl. Phys. A* **656**, 3 (1999).
- [21] O. Clarkson, F. Herwig, and M. Pignatari, Pop III i-
 process nucleosynthesis and the elemental abundances of
 SMSS J0313-6708 and the most iron-poor stars, *MNRAS*
474, L37 (2018).
- [22] M. Freer, H. Horiuchi, Y. Kanada-En'yo, D. Lee, and
 U. Meißner, Microscopic clustering in light nuclei, *Rev.*
Mod. Phys. **90**, 035004 (2018).
- [23] G. R. Caughlan and W. A. Fowler, Thermonuclear reac-
 tion rates V, *Atomic Data and Nuclear Data Tables* **40**,
 283 (1988).
- [24] H. Lorenz-Wirzba, *Untersuchung von (p, α) Reak-*
tionen Unterhalb der Coulombbarriere, Ph.D. thesis,
 Westfälischen Wilhelms-Universität zu Münster (1978).
- [25] H. Herndl, H. Abele, G. Staudt, B. Bach, K. Grün, H. Sc-
 ribany, H. Oberhammer, and G. Raimann, Direct reac-
 tion analysis of $^{19}\text{F}(p, \alpha)^{16}\text{O}$ below the Coulomb barrier,
Phys. Rev. C **44**, R952 (1991).
- [26] R. Ott, *Die Astrophysikalischen Reaktionsraten der Reak-*
tionen $^{19}\text{F}(p, \alpha)^{16}\text{O}$ und $^{19}\text{F}(p, \gamma)^{20}\text{Ne}$, Ph.D. thesis, In-
 stitut für Strahlenphysik der Universität Stuttgart (1997).
- [27] S. Dababneh, K. Toukan, and I. Khubeis, Excitation
 function of the nuclear reaction $^{19}\text{F}(p, \alpha\gamma)^{16}\text{O}$ in the pro-
 ton energy range 0.33-0 MeV, *Nuclear Instruments and
 Methods in Physics Research Section B: Beam Interac-*
tions with Materials and Atoms **83**, 319 (1993).
- [28] K. Spyrou, C. Chronidou, S. Harissopulos, S. Kossion-
 ides, and T. Paradellis, Cross section and resonance
 strengths of the $^{19}\text{F}(p, \alpha\gamma)^{16}\text{O}$ reaction in the energy
 range $E_p = 0.83-6$ MeV, *Zeitschrift für Physik A Hadrons
 and Nuclei* **357**, 283 (1997).
- [29] K. Spyrou, C. Chronidou, S. Harissopulos, S. Kossion-
 ides, T. Paradellis, C. Rolfs, W. Schulte, and L. Borucki,
 Cross section and resonance strength measurements of
 $^{19}\text{F}(p, \alpha\gamma)^{16}\text{O}$ at $E_p = 200800$ keV, *The European Phys-*
ical Journal A - Hadrons and Nuclei **7**, 79 (2000).
- [30] A. Couture, M. Beard, M. Couder, J. Görres, L. Lamm,
 P. J. LeBlanc, H. Y. Lee, S. O'Brien, A. Palumbo,
 E. Stech, E. Strandberg, W. Tan, E. Uberseder,
 R. Azuma, C. Ugalde, and M. Wiescher, Measurement

- of the $^{19}\text{F}(p, \gamma)^{20}\text{Ne}$ reaction and interference terms from $E_{c.m.} = 200\text{--}760$ keV, *Phys. Rev. C* **77**, 015802 (2008).
- [31] I. Lombardo, D. Dell'Aquila, L. Campajola, E. Rosato, G. Spadaccini, and M. Vigilante, Analysis of the $^{19}\text{F}(p, \alpha_0)^{16}\text{O}$ reaction at low energies and the spectroscopy of ^{20}Ne , *Journal of Physics G: Nuclear and Particle Physics* **40**, 125102 (2013).
- [32] I. Lombardo, D. Dell'Aquila, A. D. Leva, I. Indelicato, M. L. Cognata, M. L. Commara, A. Ordine, V. Rigato, M. Romoli, E. Rosato, G. Spadaccini, C. Spitaleri, A. Tumino, and M. Vigilante, Toward a reassessment of the $^{19}\text{F}(p, \alpha_0)^{16}\text{O}$ reaction rate at astrophysical temperatures, *Physics Letters B* **748**, 178 (2015).
- [33] M. LaCognata, A. M. Mukhamedzhanov, C. Spitaleri, I. Indelicato, M. Aliotta, V. Burjan, S. Cherubini, A. Coc, M. Gulino, Z. Hons, G. G. Kiss, V. Kroha, L. Lamia, J. Mrázek, S. Palmerini, Š. Piskoř, R. G. Pizzone, S. M. R. Puglia, G. G. Rapisarda, S. Romano, M. L. Sergi, and A. Tumino, The Fluorine destruction in stars: first experimental study of the $^{19}\text{F}(p, \alpha_0)^{16}\text{O}$ reaction at astrophysical energies, *The Astrophysical Journal* **739**, L54 (2011).
- [34] M. LaCognata, S. Palmerini, C. Spitaleri, I. Indelicato, A. M. Mukhamedzhanov, I. Lombardo, and O. Trippella, Updated THM astrophysical factor of the $^{19}\text{F}(p, \alpha)^{16}\text{O}$ reaction and influence of new direct data at astrophysical energies, *The Astrophysical Journal* **805**, 128 (2015).
- [35] I. Indelicato, M. L. Cognata, C. Spitaleri, V. Burjan, S. Cherubini, M. Gulino, S. Hayakawa, Z. Hons, V. Kroha, L. Lamia, M. Mazzocco, J. Mrazek, R. G. Pizzone, S. Romano, E. Strano, D. Torresi, and A. Tumino, New Improved Indirect Measurement of the $^{19}\text{F}(p, \alpha)^{16}\text{O}$ Reaction at Energies of Astrophysical Relevance, *The Astrophysical Journal* **845**, 19 (2017).
- [36] K. Suboti, R. Ostogi, and B. Stepani, Study of the $^{19}\text{F}(p, \gamma)^{20}\text{Ne}$ radiative capture reaction from 0.21.2 MeV, *Nuclear Physics A* **331**, 491 (1979).
- [37] G. K. Farney, H. H. Givin, B. D. Kern, and T. M. Hahn, High-energy gamma rays from the proton bombardment of fluorine, *Phys. Rev.* **97**, 720 (1955).
- [38] L. Keszthelyi, I. Berkes, I. Demeter, and I. Fodor, Resonances in $\text{F}^{19}+p$ reactions at 224 and 340 keV proton energies, *Nuclear Physics* **29**, 241 (1962).
- [39] I. Berkes, I. Dzsai, I. Fodor, and L. Keszthelyi, The resonance at 483 and 597 keV proton energies in $\text{F}^{19}+p$ reactions, *Nuclear Physics* **43**, 103 (1963).
- [40] R. R. Betts, H. T. Fortune, and R. Middleton, Structure of ^{20}Ne : The $^{19}\text{F}(^3\text{He}, d)^{20}\text{Ne}$ reaction, *Phys. Rev. C* **11**, 19 (1975).
- [41] M. Kiouss, *Détermination de taux de réactions nucléaires conduisant à la nucléosynthèse stellaire du Fluor*, Ph.D. thesis, Université de Paris-Sud (1990).
- [42] A. M. Lane and R. G. Thomas, R -matrix theory of nuclear reactions, *Rev. Mod. Phys.* **30**, 257 (1958).
- [43] D. Tilley, H. Weller, and C. Cheves, Energy levels of light nuclei $A = 16\text{--}17$, *Nuclear Physics A* **564**, 1 (1993).
- [44] I. Lombardo, D. Dell'Aquila, J.-J. He, G. Spadaccini, and M. Vigilante, New analysis of $p+^{19}\text{F}$ reactions at low energies and the spectroscopy of natural-parity states in ^{20}Ne , *Phys. Rev. C* **100**, 044307 (2019).
- [45] D. Dieumegard, B. Maurel, and G. Amsel, Microanalysis of Fluorine by nuclear reactions: I. $^{19}\text{F}(p, \alpha_0)^{16}\text{O}$ and $^{19}\text{F}(p, \alpha\gamma)^{16}\text{O}$ reactions, *Nuclear Instruments and Methods* **168**, 93 (1980).
- [46] W. B. McLean, A. Ellett, and J. A. Jacobs, The distribution in angle of the long range alpha-particles from fluorine bombarded with protons, *Phys. Rev.* **58**, 500 (1940).
- [47] G. Breuer, Messung und Analyse von Winkelverteilung und Wirkungsquerschnitt der Reaktion $\text{F}^{19}(p, \alpha_0)\text{O}^{16}$ im Energiebereich 0,4 bis 0,72 MeV, *Zeitschrift für Physik* **154**, 339 (1959).
- [48] A. Isoya, H. Ohmura, and T. Momota, The angular distributions of the long-range alpha-particles from the reaction $\text{F}^{19}(p, \alpha_0)\text{O}^{16}$, *Nuclear Physics* **7**, 116 (1958).
- [49] R. Caracciolo, P. Cuzzocrea, A. D. Rosa, G. Inghima, E. Perillo, M. Sandoli, and G. Spadaccini, The 13.645 MeV state in ^{20}Ne , *Lettere al Nuovo Cimento* **11**, 33 (1974).
- [50] S. Devons, G. Goldring, and G. R. Lindsey, Emission of Electron-Positron Pairs from Light Nuclei I: Monopole Transition in ^{16}O , *Proceedings of the Physical Society. Section A* **67**, 134 (1954).
- [51] S. Devons, M. G. N. Hine, and O. R. Frisch, The angular distribution of γ -radiation from light nuclei I. Experimental, *Proceedings of the Royal Society of London. Series A. Mathematical and Physical Sciences* **199**, 56 (1949).
- [52] S. Croft, The absolute yield, angular distribution and resonance widths of the 6.13, 6.92 and 7.12 MeV photons from the 340.5 keV resonance of the $^{19}\text{F}(p, \alpha\gamma)^{16}\text{O}$ reaction, *Nuclear Instruments and Methods in Physics Research Section A: Accelerators, Spectrometers, Detectors and Associated Equipment* **307**, 353 (1991).
- [53] T. S. Webb, F. B. Hagedorn, W. A. Fowler, and C. C. Lauritsen, Elastic Scattering of Protons by F^{19} , *Phys. Rev.* **99**, 138 (1955).
- [54] D. Tilley, C. Cheves, J. Kelley, S. Raman, and H. Weller, Energy levels of light nuclei, $A = 20$, *Nuclear Physics A* **636**, 249 (1998).
- [55] G. Caskey, Natural parity states of ^{20}Ne for $12 < E_x < 15.5$ MeV, *Phys. Rev. C* **31**, 717 (1985).
- [56] M. K. Mehta, W. E. Hunt, and R. H. Davis, Scattering of Alpha Particles by Oxygen. II. Bombarding Energy Range 10 to 19 MeV, *Phys. Rev.* **160**, 791 (1967).
- [57] H. Costantini, R. J. deBoer, R. E. Azuma, M. Couder, J. Görres, J. W. Hammer, P. J. LeBlanc, H. Y. Lee, S. O'Brien, A. Palumbo, E. C. Simpson, E. Stech, W. Tan, E. Uberseder, and M. Wiescher, $^{16}\text{O}(\alpha, \gamma)^{20}\text{Ne}$ S factor: Measurements and R -matrix analysis, *Phys. Rev. C* **82**, 035802 (2010).
- [58] E. Berthoumieux, B. Berthier, C. Moreau, J. Gallien, and A. Raoux, Parameterization of nuclear reactions cross section using R -matrix theory, *Nuclear Instruments and Methods in Physics Research Section B: Beam Interactions with Materials and Atoms* **136-138**, 55 (1998), ion Beam Analysis.
- [59] D. K. Nauruzbayev, V. Z. Goldberg, A. K. Nurmukhanbetova, M. S. Golovkov, A. Volya, G. V. Rogachev, and R. E. Tribble, Structure of ^{20}Ne states in resonance $^{16}\text{O} + \alpha$ elastic scattering, *Phys. Rev. C* **96**, 014322 (2017).
- [60] S. Hao, C. Huansheng, T. Jiayong, and Y. Fujia, Evaluation of non-rutherford cross sections, *Nuclear Instruments and Methods in Physics Research Section B: Beam Interactions with Materials and Atoms* **90**, 593 (1994).
- [61] C. M. Laymon, K. D. Brown, and D. P. Balamuth, $[^{16}\text{O}(0_2^+) + \alpha]$ parentage of continuum levels in ^{20}Ne , *Phys. Rev. C* **45**, 576 (1992).
- [62] K. L. Laursen, O. S. Kirsebom, H. O. U. Fynbo,

- 1336 A. Jokinen, M. Madurga, K. Riisager, A. Saastamoinen, 1372
 1337 O. Tengblad, and J. Äystö, High-statistics measurement 1373
 1338 of the β -delayed α spectrum of ^{20}Na , The European 1374
 1339 Physical Journal A **49**, 79 (2013). 1375
- 1340 [63] W. Huang, X. Xu, R. Ma, Z. Hu, J. Guo, Y. Guo, H. Liu, 1376
 1341 and L. Xu, Decay study of ^{20}Na and its beta-delayed ^{16}O 1377
 1342 recoiling, Science in China Series A: Mathematics **40**, 638 1378
 1343 (1997). 1379
- 1344 [64] R. E. Azuma, E. Uberseder, E. C. Simpson, C. R. Brune, 1380
 1345 H. Costantini, R. J. de Boer, J. Görres, M. Heil, P. J. 1381
 1346 LeBlanc, C. Ugalde, and M. Wiescher, AZURE: An R - 1382
 1347 matrix code for nuclear astrophysics, Phys. Rev. C **81**, 1383
 1348 045805 (2010). 1384
- 1349 [65] E. Uberseder and R. J. deBoer, *AZURE2 User Manual* 1385
 1350 (2015). 1386
- 1351 [66] C. R. Brune, Alternative parametrization of R -matrix 1387
 1352 theory, Phys. Rev. C **66**, 044611 (2002). 1388
- 1353 [67] C. R. Brune and R. J. deBoer, Secondary γ -ray decays 1389
 1354 from the partial-wave T matrix with an R -matrix ap- 1390
 1355 plication to $^{15}\text{N}(p, \alpha_1\gamma)^{12}\text{C}$, Phys. Rev. C **102**, 024628 1391
 1356 (2020). 1392
- 1357 [68] G. Audi, A. Wapstra, and C. Thibault, The Ame2003 1393
 1358 atomic mass evaluation: (II). Tables, graphs and refer- 1394
 1359 ences, Nucl. Phys. A **729**, 337 (2003), the 2003 1395
 1360 {NUBASE} and Atomic Mass Evaluations. 1396
- 1361 [69] J.-J. He, I. Lombardo, D. Dell'Aquila, Y. Xu, L.-Y. 1397
 1362 Zhang, and W.-P. Liu, Thermonuclear $^{19}\text{F}(p, \alpha_0)^{16}\text{O}$ re- 1398
 1363 action rate, Chinese Physics C **42**, 015001 (2018). 1399
- 1364 [70] H. W. Becker, W. E. Kieser, C. Rolfs, H. P. Trautvetter, 1400
 1365 and M. Wiescher, Resonance strengths of some light nu- 1401
 1366 clei, Zeitschrift für Physik A Atoms and Nuclei **305**, 319 1402
 1367 (1982). 1403
- 1368 [71] R. M. Sinclair, Gamma radiation from certain nuclear 1404
 1369 reactions, Phys. Rev. **93**, 1082 (1954). 1405
- 1370 [72] T. W. Bonner and J. E. Evans, Resonances in the disin-
 1371 tegration of fluorine and lithium by protons, Phys. Rev. **73**, 666 (1948).
- [73] C. Y. Chao, A. V. Tollestrup, W. A. Fowler, and C. C. Lauritsen, Low energy alpha-particles from fluorine bombarded by protons, Phys. Rev. **79**, 108 (1950).
- [74] D. Zahnw, C. Angulo, C. Rolfs, S. Schmidt, W. H. Schulte, and E. Somorjai, The $S(E)$ factor of $^7\text{Li}(p, \gamma)^8\text{Be}$ and consequences for $S(E)$ extrapolation in $^7\text{Be}(p, \gamma_0)^8\text{B}$, Z. Physik A - Hadrons and Nuclei **351**, 229 (1995).
- [75] D. Ezer and A. G. W. Cameron, The Evolution of Hydrogen-Helium Stars, Astrophysics and Space Science **14**, 399 (1971).
- [76] R. H. Cyburt, B. D. Fields, K. A. Olive, and T.-H. Yeh, Big bang nucleosynthesis: Present status, Reviews of Modern Physics **88**, 015004 (2016), arXiv:1505.01076 [astro-ph.CO].
- [77] M. Pignatari, F. Herwig, R. Hirschi, M. Bennett, G. Rockefeller, C. Fryer, F. X. Timmes, C. Ritter, A. Heger, S. Jones, U. Battino, A. Dotter, R. Trappitsch, S. Diehl, U. Frischknecht, A. Hungerford, G. Magkotsios, C. Travaglio, and P. Young, NuGrid Stellar Data Set. I. Stellar Yields from H to Bi for Stars with Metallicities $Z = 0.02$ and $Z = 0.01$, Astrophysical Journal Supplemental Series **225**, 24 (2016), arXiv:1307.6961 [astro-ph.SR].
- [78] R. H. Cyburt, A. M. Amthor, R. Ferguson, Z. Meisel, K. Smith, S. Warren, A. Heger, R. D. Hoffman, T. Rauscher, A. Sakharuk, H. Schatz, F. K. Thielemann, and M. Wiescher, The JINA REACLIB Database: Its Recent Updates and Impact on Type-I X-ray Bursts, The Astrophysical Journal Supplement Series **189**, 240 (2010).
- [79] M. Limongi and A. Chieffi, Presupernova Evolution and Explosive Nucleosynthesis of Zero Metal Massive Stars, The Astrophysical Journal Supplement **199**, 38 (2012), arXiv:1202.4581 [astro-ph.SR].